New insights into stress changes before and after the Wenchuan Earthquake using hydraulic fracturing measurements

Chenghu Wang [a,*], Chengke Song [b], Qiliang Guo [a], Jizhen Mao [a], Yanshan Zhang [a]

[a] Key Laboratory of Crustal Dynamics, Institute of Crustal Dynamics, China Earthquake Administration, Beijing 100085, China
[b] First Crust Deformation Monitoring and Application Center, China Earthquake Administration, Tianjin 300180, China

ABSTRACT

This paper summarizes in situ stress data by hydraulic fracturing method over the past 10 years along the Longmenshan fault belt, and these data can be divided into three segments: northern, middle, and southern. The orientations of the maximum horizontal stress rotate from north-northwest in the northern to northwest in the middle, and to west-northwest in the southern. The stress magnitudes are characterized by higher values in the two ends and lower values in the middle segment. Furthermore, three stress measurement campaigns in two boreholes on the northern segment of the Longmenshan fault belt, before and after the great earthquake, show clear stress decrease of 23%–29% in the shallow crust after the earthquake. Analysis using the mathematical fitting method also indicates a decrease in regional stress state after the earthquake. Meanwhile, the frictional characteristic indexes based on the stress measurements further imply that the frictional strength of the Longmenshan fault belt is characterized by a strong southern segment, a weak middle segment, and a moderately strong northern segment. The analysis based on the stress data implies that the northern and southern segments of the fault belt are extremely important stress concentration and transformation nodes of the regional stress regime.

1. Introduction

Great earthquakes often occur in the locked segment of active fault belts that have accumulated high stresses (Aki, 1984). The manner in which the segment with stress buildup and possible seismogenic information in a fault belt is determined is critical for predicting medium-to-long-term earthquake risks. Wiemer and Wyss (1997, 2000), Wyss and Matsumura (2002), and Wyss et al. (2000) utilized the parameters that define the relation between magnitude and frequency to analyze the spatial distribution of the relative stress level along an active fault and to identify the areas with the highest stress buildup. Diao et al. (2011) analyzed the changes in tectonic stress regimes prior to the 2008 Wenchuan Earthquake and the 1999 Chi-Chi Earthquake using focal mechanism data of Ms 4.0–6.0 earthquakes, and observed that similar local stress regime transformations occurred before both earthquakes, suggesting that this phenomenon may be a precursor to intense earthquakes. The calculation of the increase/decrease in coulomb failure stress (CFS) is another way to analyze stress changes after a strong earthquake and the earthquake's positive or negative effects on neighboring faults (King et al., 1994; Lin and Stein, 2004).

Findings from the World Stress Map (WSM) program show that the in situ stress data from the shallow crust agree well with focal mechanism data from the deep crust. Many studies worldwide (Li and Liu, 1986; Tanaka, 1986; Zoback, 1992; Zoback and Magee, 1991) have demonstrated that the direction of contemporary tectonic stress over a large region is relatively stable. Furthermore, the directions indicate a certain law and are closely related to geological structures and present tectonic movements, which is the basis for utilizing in situ stress data to explore the potential relation between tectonic stresses and earthquakes. By analyzing in situ stress measurements obtained from the shallow crust (depth < 50 m) after the Xintai, Haicheng, Longling, and Tangshan earthquakes, Li and Liu (1986) and Xie et al. (2003) observed that the principal and shear stresses of the epicentral area were considerably lower than those of adjacent areas, and that the maximum shear stresses obtained at locations far from the epicenter were up to two times greater than those in the epicentral area. The orientation of the maximum horizontal principal stress measured at the epicentral area shortly after the Tangshan Earthquake deviated considerably from the orientation of the regional tectonic stress; however, later, the two orientations were consistent (Li and Liu, 1986). Liao et al. (2003) captured the stress changes on the seismogenic fault belt shortly before and after the Kunlun Earthquake (Ms 8.1, 2001.8). Their measurements show that the stress values measured after the earthquake were only one-third of those measured before the earthquake (Liao et al., 2003). Additionally, Guo et al. (2009) obtained valuable hydraulic fracturing in situ stress measurement data

* Corresponding author at: Institute of Crustal Dynamics, CEA, P. O. 2855, No. 1 Anningzhuang Rd. Xisanqi, Haidian District, Beijing 100085, China.
E-mail address: huchengwang@163.com (C. Wang).

before and after the Wenchuan Earthquake from the same borehole. The measurements indicate a 23%–29% decrease in horizontal stress magnitudes.

Previous studies on the seismogenesis of the Wenchuan Earthquake conducted from the stress viewpoint include the systematic analysis of focal mechanism data (Cai et al., 2011; Cui et al., 2011; Hu et al., 2008), calculation of CFS (Parsons et al., 2008; Shan et al., 2009; Toda et al., 2008; Xie et al., 2010; Zhu and Wen, 2010), and variation in shear wave splitting (Ding et al., 2008). Few efforts have been made to study the Wenchuan Earthquake using in situ stress measurements. Our research group has conducted tens of hydraulic fracturing stress measurement campaigns along the Longmenshan fault belt for more than 10 years. In this study, all the data were compiled to provide a new approach to enhance our understanding of the stress changes along the Longmenshan fault belt and of the seismogenic mechanisms leading to the Wenchuan Earthquake.

2. Geological background of the Longmenshan fault belt

The Longmenshan fault belt, which has a very complicated structure, is the boundary belt between the Bayan Har Block in the Tibetan Plateau and the South China Block in the eastern China. The fault belt experienced a very long geological evolution. With a 500 km length, the Longmenshan fault belt strikes NE–SW, extending southwestward to the Jinpingshan thrust nappe belt and northeastward to join the Qingling orogenic belt. The fault belt comprises four nearly parallel faults: the Guanxian–Anxian fault in the southeastern part, the Yinxiu–Beichuan fault in the central part, the Wenchuan–Maoxian fault in the northwestern part, and the Qingchuan fault. Among these faults, the Guanxian–Anxian fault is the southeastern most boundary fault of the Longmenshan fault belt; the Yinxiu–Beichuan fault is a major fault, also called the central fault; and the Wenchuan–Maoxian and Qingchuan faults are boundary faults on the northwestern side. The eastern and western sides comprise the Sichuan Basin and the Songpan–Ganzi orogenic belt (Deng et al., 1994).

Seismological observations show that the movement intensity of the Longmenshan fault belt has been relatively weak since the Late Pleistocene epoch (i.e., during the last ten thousand years). The Holocene thrust slip speed of the western faults of the Longmenshan fault belt is 0.5–0.7 mm/a, and the right-lateral slip speed since the Late Pleistocene epoch is 0.8–1.0 mm/a (Ma et al., 2005; Tang and Han, 1993). The vertical slip speed of the central fault is 1 mm/a, and the movement intensity of the eastern faults is similar to that of the central fault (Deng et al., 1994). During the early and middle Pleistocene, the northern faults of the Longmenshan fault belt were active; however, these faults have not moved since the Late Pleistocene epoch, particularly after the middle of the Late Pleistocene epoch (Li et al., 2004). The above findings agree with those obtained by Densmore et al. (2007) and Zhou et al. (2007), who determined that the Yinxiu–Beichuan fault moves at a thrust speed of 0.3–0.6 mm/a with a right lateral slip speed of 1.0 mm/a, and that the Guanxian–Jiangyou fault moves with a thrust rate of 0.2 mm/a. Therefore, the vertical and horizontal slip speeds of the Longmenshan fault belt do not exceed 3 mm/a.

Historical and instrumental earthquake records show that there were five strong earthquakes of more than Ms 6.0 along the Longmenshan fault belt (Zhang et al., 2009a,b, 2010), and no earthquakes greater than Ms 7.0 since the beginning of documented Chinese history. However, historical earthquake records indicating that an earthquake greater than Ms 7.0 that may have occurred in the middle segment of the Longmenshan fault belt during the 1700 years prior to 2008 cannot be omitted (Wen et al., 2009). Evidently, the movement rate of the Longmenshan fault belt over approximately 1000 years, revealed by the intensity of historical earthquakes, was lower than that determined by the seismological observation at a scale of ten thousand years. The GPS observation results at a scale of ten years are consistent with the historical earthquake records (Gan et al., 2007; Shen et al., 2005). These results imply that

the Longmenshan fault belt was in a deadlocked state for more than 1000 years before the Wenchuan Earthquake. Additionally, a leveling survey from Aba County to Chengdu indicated that the Chuanxi Plateau was uplifted with respect to the Chengdu Plain during the 10 to 30 years before the Wenchuan Earthquake. The uplift rate peaked at 3.1 mm/a at Barkam, but the uplift rate of the Longmenshan fault belt with respect to the Chengdu Plain was less than 1 mm/a (Zhang et al., 2009a,b, 2010; Department of earthquake monitoring and prediction of CEA, 2009), as shown in Fig. 1.

3. Stress data

3.1. Method of in situ stress measurements

For civil engineering purposes, our research group has conducted tens of stress measurement campaigns along the Longmenshan fault belt for more than 10 years. The in situ stress data were obtained by hydraulic fracturing (Haimson and Cornet, 2003). Hydraulic fracturing determines the orientation of the principal stresses in planes normal to the borehole axis on the basis of the azimuth of induced hydraulic fracturing planes and the pressure of boreholes that are open and close to the hydro-fractures. The curve of the recorded borehole pressure vs. time presents the characteristic pressure parameters P_b, P_r, and P_s borehole. Finally, the horizontal stresses and tensile strength of the rocks are calculated using relevant equations (Lee and Haimson, 1989). After the hydraulic fracturing operation has been conducted over a test interval, a fracture impression is conducted for the same test interval to determine the maximum horizontal stress orientation. Several techniques are available for the interpretation and definition of the typical hydro-fracturing parameters (Amadei and Stephansson, 1997; Zang and Stephansson, 2010). As our data were obtained for civil engineering purposes, the parameter calculations and considerations are based on the suggested method (Haimson and Cornet, 2003), and the main equations are as follows:

$$P_s = S_h \tag{1}$$

$$S_H = 3P_s - P_r - P_0 \tag{2}$$

$$T_{hf} = P_b - P_r, \tag{3}$$

where S_H = maximum horizontal stress, S_h = minimum horizontal stress, P_b = breakdown pressure of fracturing, P_r = fracture reopening pressure, P_s = fracture closure pressure, P_0 = pore water pressure at the test interval, and T_{hf} = tensile strength of rock.

The vertical stress (S_V) can be estimated using the weight of the overburden rock:

$$S_V = \rho g d, \tag{4}$$

where ρ = unit density, g = gravitational acceleration, and d = depth.

Ever since the hydraulic fracturing in situ stress measurement technique was proposed by Haimson and Fairhurst (1970), research using this technique has continued (Amadei and Stephansson, 1997; Ito et al., 1999, 2006; Zang and Stephansson, 2010; Chang et al., 2014). The major drawback of this technique is its inaccurate determination of the maximum horizontal principal stress (Ito et al., 1999) due to inaccurate interpretation of the reopening pressure (P_r). According to a statistical analysis conducted in a previous study (Amadei and Stephansson, 1997), the error range of the minimum horizontal principal stress S_h is approximately 10%. On the basis of Eq. (2), the error range of the maximum horizontal principal stress S_H is up to 30%. To improve the accuracy of hydro-fracturing in situ stress measurement, Ito et al. (2010) developed a BABHY (Baby Borehole Hydraulic fracturing) test system for deep boreholes with depths greater than 2000 m. However, many hollow cylinder rock specimen tests have been conducted to replace Eq. (3) with the results of laboratory tensile strength tests (Amadei and Stephansson,
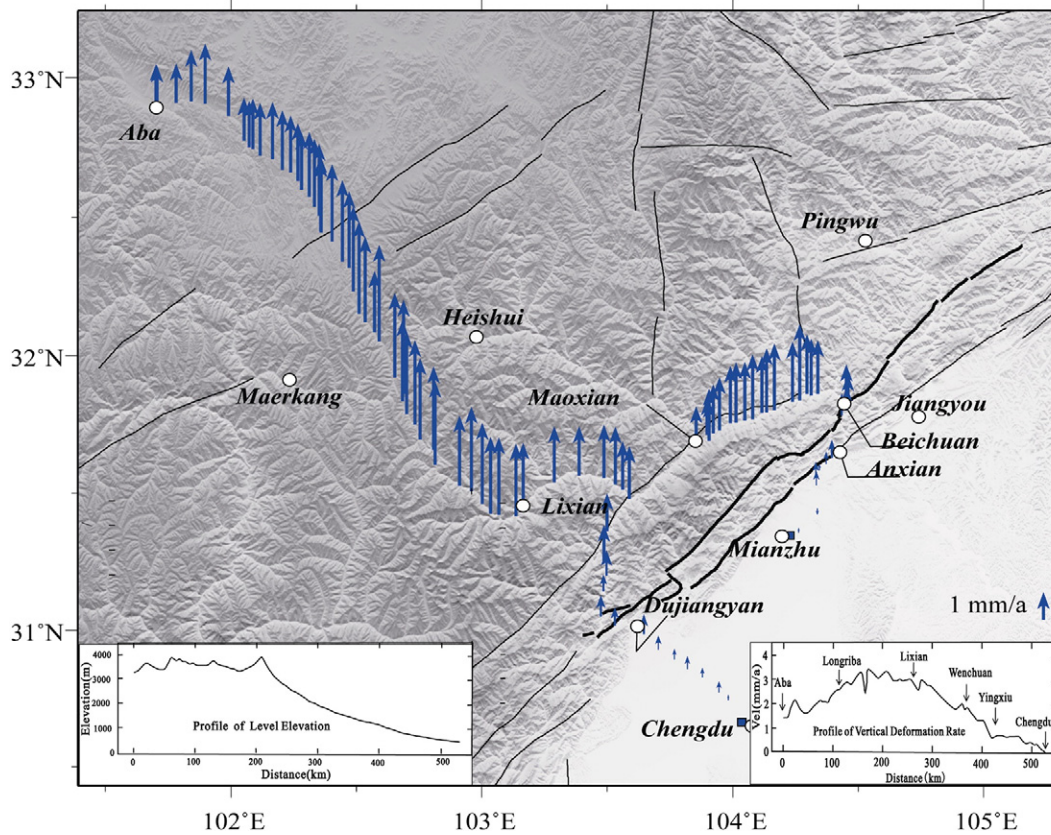
Fig. 1. Vector diagram of vertical deformation for the Longmenshan fault belt and adjacent areas. The Chengdu–Wenchuan–Aba leveling survey line represents the movement rate with respect to the reference bench 31 B of Chengdu–Miankun (1975–1997).
From Zhang et al. (2010); Department of Earthquake Monitoring and Prediction of CEA (2009).

1997; Yamashita et al., 2010; Chang et al., 2014). Nevertheless, the classic equipment, procedures and equations recommended by ISRM (Kim and Franklin, 1987) and Haimson and Cornet (2003) were adopted in this study because our measurements were obtained by different test teams over a period of ten years and the only way to ensure consistency across all teams was to follow the widely used and accepted regulations.

3.2. Description of stress data

Stress measurements for civil engineering purposes are restricted by the shallow depth of the test interval. After compilation of all the stress data, high-quality data were selected with reference to the acceptable standards. First, the data that did not have any stress orientations were not accepted, which are ranked as D in WSM (Heidbach et al., 2008). Second, only data below certain depths were selected because stress data from a shallow test interval can be affected by various factors (Haimson, 2010). Zoback (2007) suggested that in situ stress measurements conducted at depths greater than 100 m seem to be independent of nontectonic processes. Third, previous research findings for the stress regime based on seismogeological research and focal mechanism data show that the stress state in this area should be favorable for thrust or strike slip faults (Anderson, 1951). Therefore, if the stress data could not define the stress state as either of the two types expected above, the measured data were excluded. As the test depths of the data were greater than 100 m, according to the WSM data quality ranking system, the data should be ranked as category B or C.

The stress data were categorized according to the geographical locations and measurement date. The locations and stress orientations are shown in Fig. 2. These data were obtained from 29 different measurement sites. Tables 1 and 2 summarize all stress data and include the details of the lithology of the measurement sites, data quality, and initial analytical results. Among the boreholes, one was used for repeated stress measurement on the Beichuan-Yinxiu fault after the Wenchuan Earthquake; the repeated test results are also listed in Table 2.

In Tables 1 and 2, k_{Hmax}, k_{hmin}, μ_m, and R, were calculated using Eqs. (5) to (8) with the measured values of the three principal stresses. The lateral pressure coefficients in geotechnical engineering k_{Hmax} and k_{hmin} represent the ratios of the maximum and minimum horizontal principal stresses to the vertical stress. The ratio of the maximum shear stress $((\sigma_1 - \sigma_3)/2)$ to the mean effective stress $((\sigma_1 + \sigma_3) - 2P_f)/2$ (where P_f is the pore pressure) is μ_m, which agrees well with the friction coefficient predicted using the Coulomb frictional-failure theory, Eq. (9) (Zoback, 2007; Zoback and Townend, 2001). Therefore, μ_m, defined as the frictional characteristic index, has a similar physical meaning to μ (apparent friction coefficient) for optimally oriented faults with respect to Eq. (9) and Fig. 3, as demonstrated in Appendix A. Jamison and Cook (1980) compared the relation between in situ stress data and various types of fault, and observed that the fitted slope on a plot of maximum shear stress vs. average principal stress represented the Coulomb friction coefficient. Furthermore, Jamison and Cook (1980) observed that different types of faults were characterized by varying friction coefficients, which actually reflected the differences between faults. Essentially, μ_m is an indicator that reflects the stress buildup in the upper crust. According to Chang et al. (2010), for the best-fit stress model to cause a fault to slip, the value of R is estimated to be approximately 0.5, i.e., the magnitude of σ_2 is nearly the average of the magnitudes of σ_1 and σ_3.

$$k_{Hmax} = S_H/S_V \tag{5}$$

$$k_{hmin} = S_h/S_V \tag{6}$$

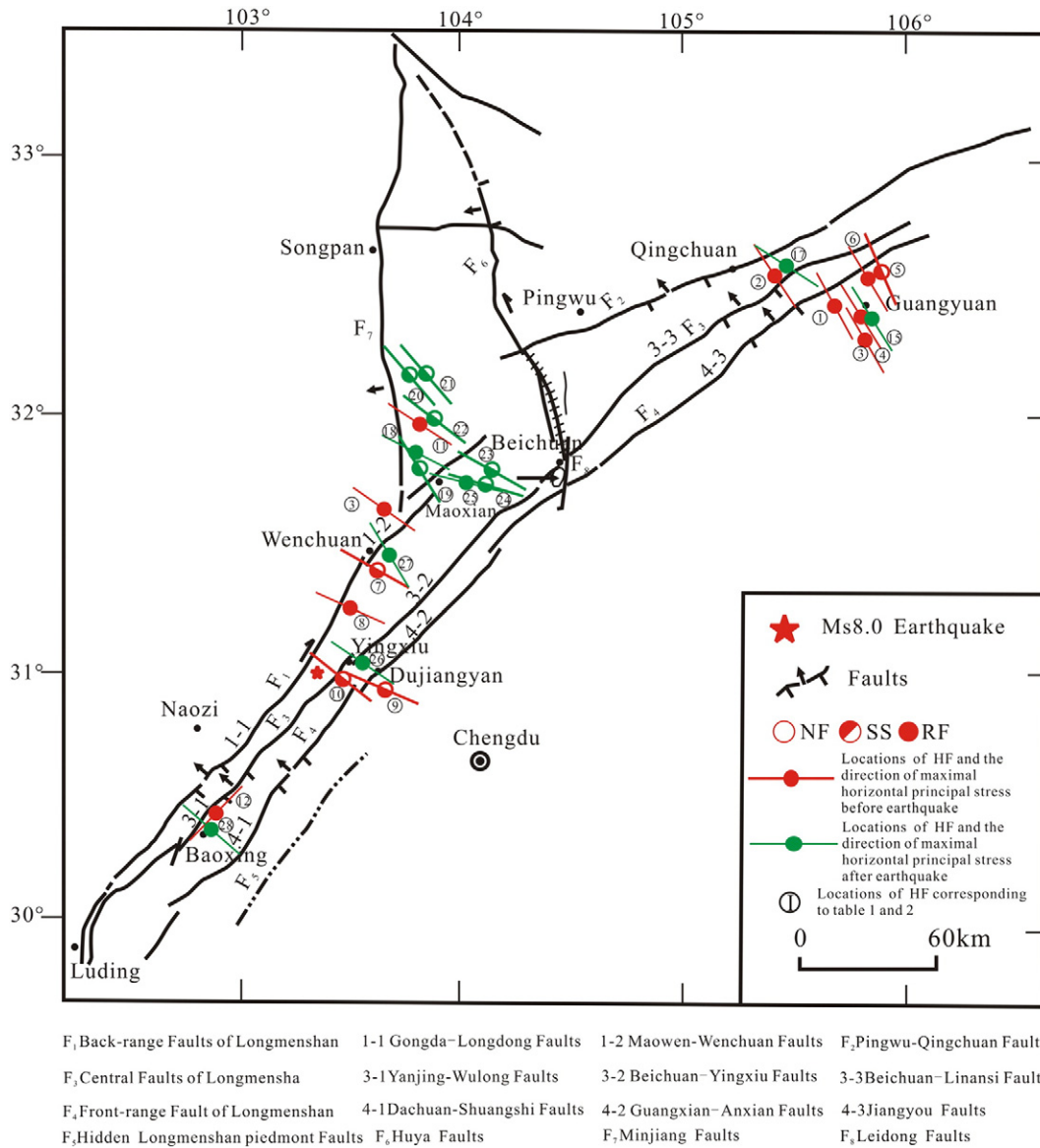$$\mu_m = (\sigma_1 - \sigma_3)/(\sigma_1 + \sigma_3 - 2P_f) \tag{7}$$

Fig. 2. Locations and stress orientations of different measurement sites.

$$R = (\sigma_2 - \sigma_1)/(\sigma_3 - \sigma_1) \tag{8}$$

$$\mu_m = \mu/\sqrt{\mu^2 + 1} \tag{9}$$

Before the Wenchuan Earthquake, most of the stress data in Table 1, which were obtained from different boreholes, were in thrust fault conditions (60%), and the remaining data were in strike slip fault conditions (40%). However, after the Wenchuan Earthquake, most measurement data were in strike slip fault conditions (58%), with a smaller amount in thrust fault conditions (42%). These results agree well with the focal mechanism and field investigation results of seismic surface ruptures of the Wenchuan Earthquake (Teng et al., 2008; Xu et al., 2009; Zhang et al., 2013).

Using the data presented in Tables 1 and 2 and the measurement locations indicated in Fig. 2, the measured in situ stress data along the Longmenshan fault belt can be divided into three segments: southern, middle, and northern. As the measurement locations are rather sparse and concentrated in these three segments, we discuss the data in terms of these three major regions. The stress orientations along the Longmenshan fault belt (shown in Fig. 2) rotate slightly from the northern to southern segment, i.e., the stress orientation alters from north-northwest in the northern segment to north-west in the middle segment, and to west-northwest (or nearly east–west) in the southern segment. From Fig. 4, the characteristic values based on the measurements can be further divided into three subgroups: southern, middle, and northern. Compared with the stress data prior to the Wenchuan Earthquake, the stress magnitudes determined after the earthquake decreased to some extent. In Section 4, the stress data before and after the earthquake will be compared and discussed with regard to the northern, middle, and southern segments. The potential geodynamic significance of the data will also be addressed.

4. Analysis of stress data

4.1. Stress changes

In this section, the geodynamic significance of the data from Tables 1 and 2 will be discussed and analyzed. In Section 3, the stress state defined by the measurements was analyzed with respect to the theory of Anderson (1951), and the stress orientations were discussed

Table 1
Summary of in-situ stress measurements along the Longmenshan fault belt before Wenchuan Earthquake.

Serial no.	Borehole name	Location	Distance (km)	Depth	Lithology	Quality	Stress state	S_H	S_h	S_V	P_0	Orientation of S_H (°)	k_{Hmax}	k_{hmin}	μ_m	R	Date of test
1	GY_B-L, ZK2	Baolun, Guangyuan	20	144	Limestone	B	RF	7.39	4.42	3.75	0.94	/	1.97	1.18	0.39	0.82	2008.4.22–4.25
				200		B	RF	12.93	7.46	5.2	1.49	/	2.49	1.43	0.51	0.71	
				256		B	RF	14.98	9.01	6.66	2.04	N32°W	2.25	1.35	0.47	0.72	
				312.8		B	RF	14.04	8.57	8.13	2.60	N25°W	1.73	1.05	0.35	0.93	
				Average								N28.5°W	2.11	1.26	0.43	0.79	
2	QC_M-Y, ZK1	Muyu, Qingchuan	7	359.53	Metamorphic phyllite	B	RF	15.8	10.03	9.35	3.25	N28°W	1.69	1.07	0.35	0.89	2008.5.04–5.07
				390.6		B	RF	21.11	12.83	10.15	3.56	N35°W	2.08	1.26	0.45	0.76	
				408.8		B	RF	21.78	13.01	10.63	3.74	/	2.05	1.22	0.45	0.79	
				417.6		B	RF	22.88	13.6	10.86	3.82	N32°W	2.11	1.25	0.46	0.77	
				Average								N31.7°W	1.98	1.20	0.43	0.80	
3	GY_S-J-P, ZK4	Shijingpu, Guangyuan	47	305	Mudstone, sand stone	B	SS	9.85	6.49	7.93	2.63	N33°W	1.24	0.82	0.30	0.57	2008.4.05–4.08
				349.5		B	SS	14.29	8.93	9.09	3.07	/	1.57	0.98	0.31	0.97	
				363		B	SS	14.52	9.26	9.44	3.2	N25°W	1.54	0.98	0.30	0.97	
				394.5		B	SS	15.23	9.87	10.26	3.51	N32°W	1.48	0.96	0.30	0.93	
				Average								N30°W	1.46	0.94	0.30	0.86	
4	GY_P-L, ZK3	Panlong, Guangyuan	30	358.9	Mudstone, sand stone	B	SS	11.02	7.52	9.33	3.52	N31°W	1.18	0.81	0.30	0.48	2008
				406.1		B	SS	11.98	8.48	10.56	3.98	N33°W	1.13	0.80	0.28	0.41	
				Average								N32°W	1.16	0.80	0.29	0.44	
5	GY_C-T	Chaotian, Guangyuan	16	328.5	Limestone	C	SS	13.45	7.97	8.53	2.24		1.58	0.93	0.32	0.90	2008
				346.8		C	SS	13.13	7.77	9.01	2.42	N23°E	1.46	0.86	0.33	0.77	
				363.8		C	SS	13.3	7.94	9.45	2.59		1.41	0.84	0.33	0.72	
				Average								N23°E	1.48	0.88	0.33	0.79	
6	GY_C-T2	Chaotian, Guangyuan	16	174.6	Limestone	B	RF	12.24	6.71	4.53	0.93		2.70	1.48	0.52	0.72	2007
				197.7		B	RF	13.1	7.56	5.13	1.15	N30°W	2.55	1.47	0.50	0.70	
				235.6		B	RF	13.47	7.93	6.12	1.52	N35°W	2.20	1.30	0.44	0.75	
				257.7		B	RF	14.31	8.15	6.69	1.74	N27°E	2.14	1.22	0.43	0.81	
				276.6		B	RF	14.12	8.34	7.18	1.93		1.97	1.16	0.40	0.83	
				Average								N30.7°W	2.31	1.33	0.46	0.76	
7	Wenchuan	Wenchuan	25	300	Sandstone	C	SS	11	7.5	7.95	2.5		1.38	0.94	0.26	0.87	2001
				348		C	SS	12.1	7	9.22	2.9	N60°W	1.31	0.76	0.38	0.56	
				390		C	SS	14	10	10.34	3.4		1.35	0.97	0.23	0.92	
				Average								N60°W	1.35	0.89	0.21	0.78	
8	WC_M-C	Mianchi, Wenchuan		290.9	Granite	B	RF	18.85	10.4	7.86	1.65	N66°W	2.40	1.32	0.47	0.77	2000
				Average								N66°W	2.40	1.32	0.47	0.77	
9	DJY-M-X	Maxi, Dujiangyan	22	389.6	Mud shale	C	SS	13.7	9.15	10.53	3.90	N66°W	1.30	0.87	0.30	0.70	2001
				394.2		C	SS	15.05	9.9	10.66	3.95	/	1.41	0.93	0.30	0.85	
				Average								N66°W	1.36	0.90	0.30	0.77	
10	WC_Y-X	Yinxiu, Wenchuan	4	246.7	Argillaceous siltstone, sandy mudstone	B	SS	7.47	4.57	6.67	0.97	/	1.12	0.69	0.29	0.28	2002
				300.0		B	SS	12.55	7.2	8.11	1.50	/	1.55	0.89	0.32	0.83	
				354.2		B	SS	13.8	8.1	9.58	2.05	/	1.44	0.85	0.32	0.74	
				422.2		B	SS	16.58	9.83	11.41	2.73	N47°W	1.45	0.86	0.32	0.77	
				476.2		B	SS	20.62	12.12	12.87	3.27	/	1.60	0.94	0.32	0.91	
				611.4		B	SS	19.17	12.42	16.51	4.62	N54°W	1.16	0.75	0.30	0.39	
				677.1		B	SS	21.23	13.43	18.29	5.28	/	1.16	0.73	0.32	0.38	
				705.7		B	SS	26.36	16.16	19.07	5.56	N53°W	1.38	0.85	0.32	0.71	
				733.2		B	SS	28.04	17.14	19.81	5.84	/	1.42	0.87	0.33	0.76	
				Average								N51.3°W	1.36	0.82	0.32	0.64	
11	MX_J-C	Jiaochang, Maoxian		247	Sandstone	B	RF	14.0	7.7	6.5	2.4	N54°W	2.15	1.18	0.48	0.84	2001
				250		B	RF	14.0	7.7	6.6	2.49	N56°W	2.12	1.17	0.47	0.85	
				252		B	RF	13.4	7.7	6.7	2.50	N60°W	2.00	1.15	0.44	0.85	
												N56.7°W	2.09	1.17	0.47	0.85	
12	BX-N-Z	Naozi, Baoxing	30	180.3	Silty phyllite	B	RF	15.42	8.28	4.77	1.08		3.23	1.74	0.59	0.67	1999
				187.6		B	RF	14.44	8.19	4.96	1.15	N57.0°E	2.91	1.65	0.55	0.66	
				224.4		B	RF	20.86	11.61	5.49	1.51	N63.0°E	3.80	2.11	0.66	0.60	
				233.3		B	RF	18.07	11.11	6.18	1.60	N1.0°W	2.92	1.80	0.56	0.59	
				250.3		B	RF	19.74	10.8	6.63	1.77	N55.0°E	2.98	1.63	0.57	0.68	
				259.1		B	RF	21.38	11.68	6.86	1.85		3.12	1.70	0.59	0.67	
				280.5		B	RF	25.53	13.53	7.42	2.06		3.44	1.82	0.63	0.66	
				Average								N58.3°	3.20	1.78	0.59	0.65	
13	YJ-L-H-K	Lianghekou, Yajiang	150?	92.4	Sandy slate, sandstone	B	RF	16.18	8.96	2.49	1.03	N74°W	6.50	3.60	0.82	0.53	2004
				101.5		B	RF	15.52	9.04	2.74	1.12	/	5.66	3.30	0.80	0.51	
				109.5		B	RF	23.2	12.62	2.96	1.20	/	7.84	4.26	0.85	0.52	
				116.4		B	RF	17.11	9.89	3.14	1.27	/	5.45	3.15	0.79	0.52	
				143.5		B	RF	17.38	9.46	3.87	1.53	/	4.49	2.44	0.74	0.59	
				147.9		B	RF	19.52	10.55	3.99	1.58	/	4.89	2.64	0.76	0.58	
				158.4		B	RF	14.67	8.55	4.28	1.68	N70°W	3.43	2.00	0.67	0.59	
				194		B	RF	19.45	10.83	5.24	2.03	/	3.71	2.07	0.69	0.61	
				228.6		B	RF	31.46	17.29	6.17	2.37	/	5.10	2.80	0.77	0.56	
				240		B	RF	20.02	11.8	6.48	2.48	/	3.09	1.82	0.63	0.61	
				Average								N72°W	5.02	2.30	0.75	0.56	

Table 2
Summary of in-situ stress measurements along the Longmenshan fault belt after Wenchuan Earthquake.

Serial no.	Borehole name	Location	Distance (km)	Depth	Lithology	Quality	Stress state	Principal stresses (MPa)				Orientation of S_H	k_{Hmax}	k_{hmin}	μ_m	R	Notes
								S_H	S_h	S_V	P_0						
14	QC_M-Y, ZK1	Muyu, Qingchuan	7	390.6	Metamorphic phyllite	C	RF	15.73	10.33	10.15	3.56	/	1.55	1.02	0.30	0.97	2008.6.26–6.29
				408.8		C	SS	15.91	10.01	10.63	3.74	/	1.50	0.94	0.32	0.89	
				417.6		C	SS	16	10.1	10.86	3.82	/	1.47	0.93	0.32	0.87	
				Average									1.51	0.96	0.31	0.91	
15	GY_P-L, ZK3	Panlong, Guangyuan	30	358.9	Mudstone, sand stone	B	SS	10.52	7.52	9.33	3.62	/	1.13	0.81	0.28	0.40	2008.6
				406.1		B	SS	11.88	8.48	10.56	4.00	/	1.13	0.80	0.28	0.39	
				Average									1.13	0.80	0.28	0.39	
16	GY-B-L2, ZK5	Baolun, Guangyuan	20	369.1	Mudstone, sandstone	D	RF	16.73	9.64	9.6	1.27		1.74	1.00	0.30	0.99	2008.5.25–5.28
				378.4		D	RF	17.07	10.49	9.84	1.36		1.73	1.07	0.30	0.91	
				Average									1.74	1.04	0.30	0.95	
17	QC_M-Y2, ZK6	Muyu, Qingchuan	7	248.2	Metamorphic phyllite	C	RF	12.99	7.94	6.46	1.89	N61°W	2.01	1.23	0.42	0.77	2008.7.2–7.5
				318.3		C	RF	15.67	9.12	8.28	2.57		1.89	1.10	0.39	0.89	
				332.3		C	RF	13.81	9.26	8.64	2.71	N53°W	1.60	1.07	0.30	0.88	
				362		C	RF	15.6	10.05	9.41	3.0		1.79	1.07	0.33	0.90	
				Average								N57°W	1.72	1.08	0.36	0.86	
18	MX_F-H	Feihong, Maoxian	60	231.2	Phyllite	C	RF	10.96	7.26	6.12	2.07	N73°W	1.79	1.19	0.37	0.76	2010
				289		C	RF	14.02	8.83	7.65	2.64		1.83	1.15	0.39	0.81	
				324.2		C	RF	15.88	9.68	8.58	2.98		1.85	1.13	0.39	0.81	
				457		C	SS	17.68	11.48	12.09	4.28	N55°W	1.46	0.95	0.30	0.90	
				485.1		C	SS	18.94	12.25	12.84	4.56		1.48	0.95	0.30	0.91	
				540		C	SS	20.48	13.29	14.28	5.10	N60°W	1.43	0.93	0.31	0.86	
				570.1		C	SS	21.29	13.59	15.08	5.39		1.41	0.90	0.22	0.81	
				Average								N62.7°W	1.61	1.03	0.33	0.84	
19	MX_F-H2	Feihong, Maoxian	60	410.7	Phyllite	C	SS	16.2	9.96	10.67	3.39		1.52	0.93	0.32	0.89	2010
				484.7		C	SS	18.09	11.65	12.59	4.11	N31°W	1.44	0.93	0.30	0.85	
				558.6		C	SS	20.38	12.91	14.51	4.84		1.40	0.89	0.32	0.79	
				595.6		C	SS	19.84	12.99	15.47	5.20	N28°W	1.28	0.84	0.31	0.64	
				743.5		C	SS	25.05	16.26	19.31	6.65	N34°W	1.30	0.84	0.31	0.65	
				Average								N31°W	1.39	0.89	0.31	0.76	
20	MX-T-P	Taiping, Maoxian	76	390.9	Phyllite	C	SS	13.25	7.84	10.35	0.4	N38°W	1.28	0.76	0.27	0.54	2010
				401.5		C	SS	15.8	8.55	10.63	0.5	N41°W	1.49	0.80	0.31	0.71	
				Average								N39.50°W	1.38	0.78	0.29	0.62	
21	MX-T-P2	Taiping, Maoxian	80	352.8	Phyllite, sandstone	C	SS	14.51	7.66	9.34	0.36	N38°W	1.55	0.82	0.32	0.75	2010
				385.0		C	SS	13.17	7.48	10.19	0.68	N41°W	1.29	0.73	0.29	0.52	
				Average								N39.50°W	1.42	0.78	0.31	0.64	
22	MX_D-X	Diexi, Maoxian	53	760.6	Phyllite, sandstone	C	SS	21.19	12.95	20.11	4.2	N52°W	1.05	0.64	0.32	0.13	2010

Table 2 (*continued*)

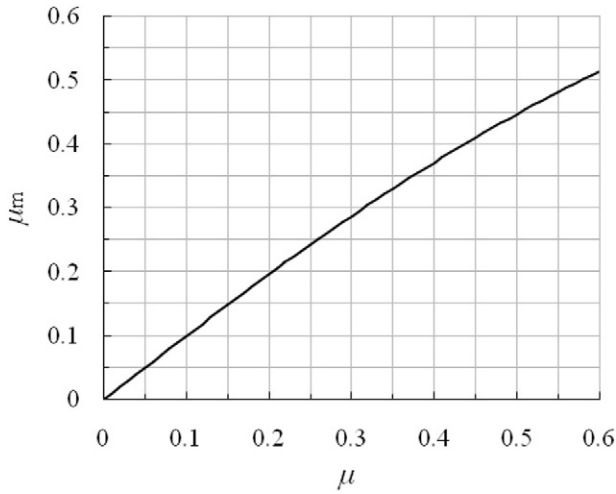| Serial no.	Borehole name	Location	Distance (km)	Depth	Lithology	Quality	Stress state	Principal stresses (MPa)				Orientation of S_H	k_{Hmax}	k_{hmin}	μ_m	R	Notes
								S_H	S_h	S_V	P_0						
				Average								N52°W	1.05	0.64	0.32	0.13	
23	MX_L-M-S	Longmenshan, Maoxian	22	352.5	Phyllite	C	SS	12.95	8.01	9.32	2.47	/	1.39	0.86	0.31	0.73	2011
				380.1		C	SS	15.25	9.28	10.05	2.75	N55°W	1.52	0.92	0.31	0.87	
				493.5		C	SS	16.74	10.76	13.05	3.85	N62°W	1.28	0.82	0.30	0.62	
				549.9		C	SS	18.02	11.4	14.55	4.40		1.24	0.78	0.32	0.52	
				578.1		C	SS	17.85	11.7	15.29	4.68		1.17	0.77	0.30	0.42	
				591.4		C	SS	17.14	11.72	15.64	4.81	N68°W	1.10	0.75	0.28	0.28	
				Average								N61.7°W	1.28	0.82	0.31	0.57	
24	MX_L-M-S2	Longmenshan, Maoxian	34	466.3	Phyllite	C	SS	15.36	10.07	12.25	4.28	N68°W	1.25	0.82	0.31	0.59	2011
				509.9		C	SS	16.3	11	13.39	4.7		1.22	0.82	0.30	0.55	
				555.5		C	SS	15.23	10.44	14.58	5.15	N75°W	1.04	0.72	0.31	0.14	
				584.0		C	SS	17.01	11.72	15.33	5.43		1.11	0.76	0.30	0.32	
				625.3		C	SS	16.43	11.63	16.42	5.83		1.00	0.71	0.29	0.00	
				656.6		C	SS	19.72	13.43	17.24	6.14		1.14	0.78	0.30	0.39	
				686.4		C	SS	20.03	13.73	18.02	5.43		1.11	0.76	0.28	0.32	
				718.3		C	SS	20.33	14.04	18.86	6.75	N82°W	1.08	0.74	0.30	0.23	
				748.8		C	SS	22.14	14.84	19.66	7.04		1.13	0.75	0.32	0.34	
				Average								N75°W	1.12	0.76	0.30	0.32	
25	MX_G-M	Guangming, Maoxian		153.79	Phyllite	C	RF	7.4	4.51	4	1.12	N75°W	1.85	1.13	0.37	0.85	2010
				172.87		C	RF	11.79	6.7	4.5	1.31	N80°W	2.62	1.49	0.53	0.70	
				184.82		C	RF	11.72	6.82	4.81	1.42	N72°W	2.44	1.42	0.50	0.71	
												N75.7°W	2.30	1.34	0.47	0.75	
26	WC_Y-X2	Yinxiu, Wenchuan	2	142	Granite	C	RF	9.81	5.95	3.76	1.34	N56°W	2.61	1.58	0.56	0.64	Wu et al., 2010
				Average								N56°W	2.61	1.58	0.56	0.64	
27	WC_B-L	Bingli, Wenchuan		165.5		B	RF	12.37	7.41	4.39	1.52	N35°W	2.82	1.69	0.58	0.62	2012
				169.2	Phyllite	B	RF	11.61	7.17	4.4	1.56	/	2.64	1.63	0.56	0.62	
				182.8		B	RF	12.66	7.48	4.75	1.69	/	2.67	1.57	0.56	0.65	
				191.5		B	RF	17.18	9.72	4.98	1.78	N27°W	3.45	1.95	0.66	0.61	
				Average								N31°W	2.89	1.71	0.59	0.63	
28	Baoxing	Baoxing		189		B	RF	12.87	7.36	5.01	1.89	N23°W	2.57	1.47	0.56	0.70	Wu et al., 2010
				219	Granite	B	RF	10.83	6.45	5.8	2.19		1.87	1.11	0.41	0.87	
				317		B	RF	18.28	11.09	8.4	3.17	N74°W	2.18	1.32	0.49	0.73	
				Average									2.20	1.30	0.48	0.77	
29	Kangding	Kangding	26	136	Granite	D	RF	5.41	3.55	3.60	1.12		1.50	0.99	0.27	1.03	Wu et al., 2010
				172		D	RF	9.81	5.92	4.56	1.48		2.15	1.30	0.46	0.74	
				186		D	RF	7.31	4.94	4.93	1.62		1.48	1.00	0.26	1.00	
				Average									1.71	1.10	0.33	0.92	

Fig. 3. Relation between the frictional characteristic index μ_m and the apparent friction coefficient μ, derived from the theory of Anderson.

statistically. However, these analyses were not sufficient to reveal the geodynamic significance of the stress data. Therefore, the modified Sheorey's model (Sheorey, 1994; Wang et al., 2009) was used to fit the measured stress data before and after the earthquake, as shown in Fig. 5. The stresses S_H and S_h were fitted to facilitate subsequent discussion. The fitting equations for k_{Hmax} and k_{hmin} based on the measured stress data before the earthquake were $k_{Hmax} = 0.71 + 494.2/Z$, $k_{hmin} = 0.49 + 259.8/Z$, and $k_{av} = 0.60 + 377.0/Z$. The fitting equations for k_{Hmax} and k_{hmin} based on the measured stress data after the earthquake were $k_{Hmax} = 0.56 + 306.1/Z$, $k_{hmin} = 0.42 + 164.1/Z$, and $k_{av} = 0.49 + 235.1/Z$.

The stress data obtained before and after the earthquake and the data-based fitting equations coincided with the range of $100/z + 0.3 < k_{av} < 1500/z + 0.5$, as suggested by Brown and Hoek (1978). At the same time, the distribution law of the stress data from the shallow crust was consistent with the findings of Batchelor (1984) and Rummel et al. (1986), which further demonstrates the reliability of the stress data used in this paper. However, for depths greater than 2 km, the results of the fitting equations were less than the ranges of $k_{Hmax} \approx 1.0$ and $k_{hmin} \approx 0.5$ given by Rummel et al. (1986). Batchelor (1984) suggested that the distribution law of stresses in the hot and dry granite of Cornwall should be $k_{Hmax} = 580/Z + 1.06$ and $k_{hmin} = 150/z + 0.5$. However, under such stress conditions, fluid injected into a 3-km-deep borehole induced micro-earthquakes in the

rock mass, indicating that the stress state was that of critical equilibrium. Comparing the fitting equations based on hydraulic fracturing measurements before and after the Wenchuan earthquake, the stress state after the earthquake decreased significantly. Assuming that the depth is equal to 1 km, the values of S_H and S_h calculated with the fitting equations before the earthquake were 31.9 and 19.9 MPa, respectively. However, S_H and S_h calculated with the fitting equations after the earthquake were 22.9 and 15.5 MPa, indicating a decrease of 28.2% and 22.1%, respectively. The fitting equations are based on stress data from tens of measurement campaigns and therefore represent the stress state of the entire region along the Longmenshan fault belt. The result of the comparison thus implies a decrease in the tectonic stress field in this area after the earthquake. Because of the fitting parameters, the fitting equations may be influenced by the mathematical model or other factors. The stress decrease reflected by the fitting equations must therefore be confirmed by further research or alternative methods.

After discussing the entire regional stress state, the method of Zoback and Townend (2001) was applied to the measured stress data to analyze the relation between maximum shear stress and mean normal stress. Data from before and after the earthquake (Tables 1 and 2) are plotted on Fig. 6(a) and (b), respectively. From Fig. 5(a), before the earthquake, data from one point of the southern segment fall in the range constrained by $\mu = 0.6$–1.0 through Byerlee's law. Furthermore, data from another point of the southern segment were beyond the range set by $\mu = 1.0$, and data from the middle and northern segments were within the range constrained by $\mu = 0.2$–0.6. Although the stress state based on measurements did not reach the limit defined by $\mu = 0.6$ (Zoback and Townend, 2001), the Wenchuan Earthquake struck the middle and northern segments of the Longmenshan fault belt. As shown in Fig. 5(b), after the earthquake, most data fall in the range defined by $\mu = 0.2$–0.6; however, data from two points of the middle segment and one point of the southern segment were within the range defined by $\mu = 0.6$–1.0. According to the Byerlee's law, the whole stress state of this area did not reach the lower limit of frictional slip, but there was an intense earthquake in this area. This implies a low frictional strength of the Longmenshan fault. In accordance with the theoretical deduction in Appendix A, μ_m calculated with the measured stresses was similar to μ. Therefore, the μ_m values of different segments along the Longmenshan fault belt were calculated. The μ_m values for the southern, middle, and northern segments calculated using pre-earthquake data (Table 1), were 0.67, 0.35, and 0.36, respectively, which have the same geodynamic meaning as Fig. 6(a). The μ_m values of the southern, middle, and northern segments calculated using postearthquake (Table 2) were 0.41, 0.37, and 0.31, respectively, which have the same geodynamic meaning as Fig. 6(b). If the postearthquake data from two points in the
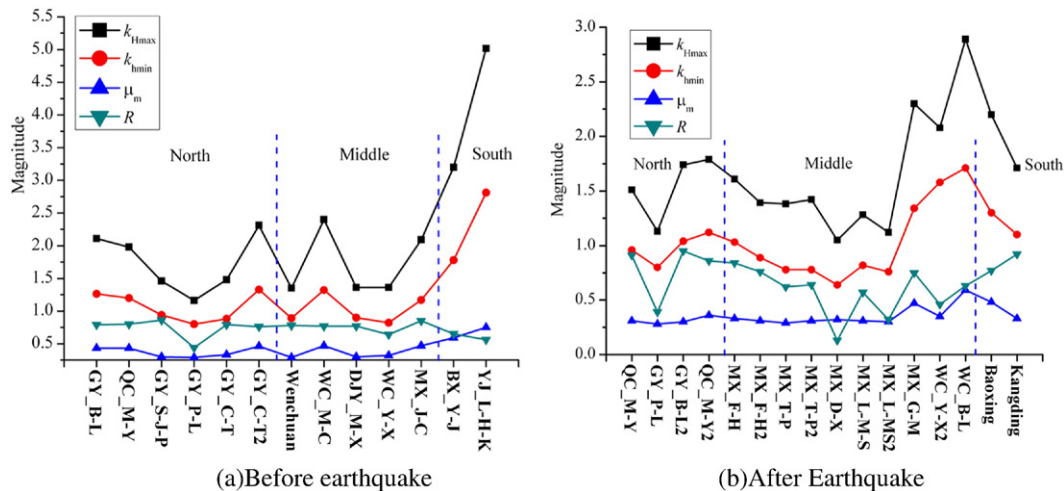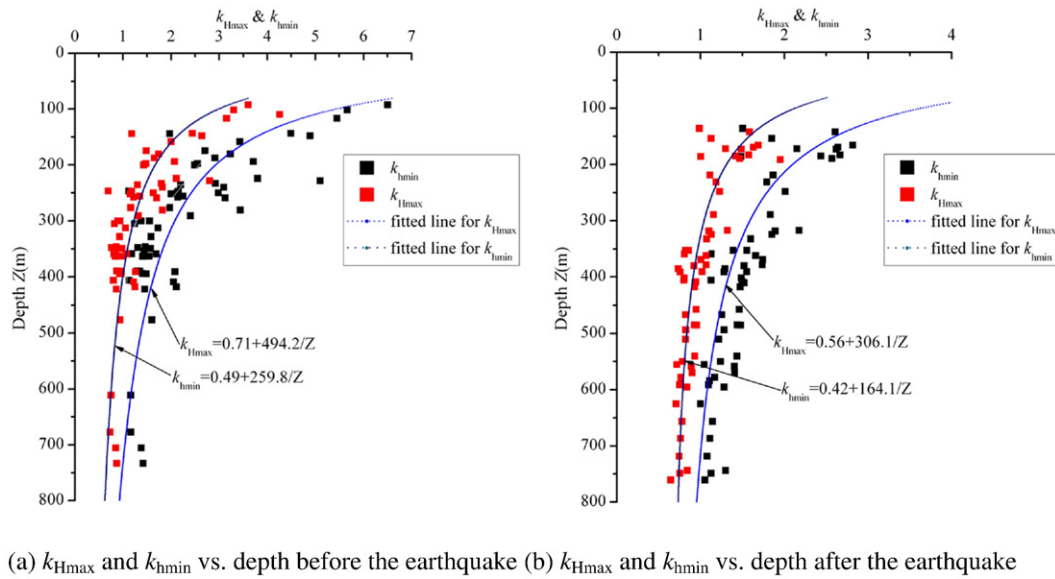

(a)Before earthquake

(b)After Earthquake

Fig. 4. Stress status of different measurement sites before and after the Wenchuan Earthquake.

(a) k_{Hmax} and k_{hmin} vs. depth before the earthquake (b) k_{Hmax} and k_{hmin} vs. depth after the earthquake

Fig. 5. Lateral pressure coefficients vs. depth of all stress measurements before and after the Wenchuan Earthquake. (a) k_{Hmax} and k_{hmin} vs. depth before the earthquake (b) k_{Hmax} and k_{hmin} vs. depth after the earthquake.

middle segment with totally different lithologies were excluded, the μ_m for the middle segment would be 0.31 for the middle segment. Based on its defining equation, μ_m not only reflects the frictional property of regional faults but also indicates the stress buildup of a single area. Correspondingly, when all μ_m values calculated from the stress data before and after the earthquake were averaged, the mean μ_m values along the Longmenshan fault belt are 0.46 (pre-earthquake) and 0.36 (postearthquake). The percentage decrease in mean μ_m after the earthquake was 22%, which is similar to that determined by the fitting equation. The geodynamic meaning of μ_m will be discussed in detail below.

4.2. Repeated measurements after the earthquake

The Wenchuan Earthquake occurred abruptly, and most scientists did not make any psychological or disaster relief preparations prior to this great earthquake. Fortunately, during April and May 2008, before the Wenchuan Earthquake, four hydraulic fracturing in situ stress measurement campaigns were conducted by our research group in Qingchuan and Guangyuan prefectures in the northern segment of the Longmenshan fault belt. In particular, a stress measurement campaign was completed on May 6, 2008 for borehole QC-M-Y, which is located in the mountainous area of Muyu village, Qingchuan County, 7 km from the seismogenic fault. This borehole was in the hanging wall of the seismogenic fault, and three other boreholes were in the footwall of the fault belt (as indicated in Fig. 2). After the Wenchuan Earthquake, a hydraulic fracturing stress measurement campaign was conducted in borehole QC_M-Y2, which is adjacent to borehole QC_M-Y, and the stress measurement campaign was repeated in borehole QC_M-Y to study the change in the in situ stresses before and after the earthquake. For the repeated stress measurement campaign in borehole QC_M-Y, the test and calculation procedures followed the principles set up by Haimson and Cornet (2003). Actually, the repeated stress measurement was performed as per the hydraulic fracturing tests on pre-existing fractures, i.e., the pre-induced hydraulic fractures were reopened at the same test interval in the same borehole after the earthquake. The stress measurement results are presented in Tables 1 and 2.

The original testing records before and after the earthquake in borehole QC_M-Y on the seismogenic fault belt are shown in Fig. 7. The recording curves are quite typical, and the characteristic hydraulic fracturing parameters, particularly the fracture closure pressure (i.e., the minimum horizontal principal stress), are quite clear and definite on

the recording curves. Therefore, the measured results are considered to be accurate and reliable, and can truly represent the in situ stress state at the testing site (Amadei and Stephansson, 1997).

The comparison of the pre-earthquake and postearthquake stress measurement data from borehole QC_M-Y showed that the stress magnitude decreased significantly and the changes in the maximum and minimum horizontal stresses at a depth of 408.80 m were 5.87 and 3 MPa, respectively. The values of k_{Hmax}, k_{hmin}, and μ_m determined after the earthquake decreased by 24%, 21.7%, and 28%, respectively, compared with the pre-earthquake values, similar to the previous results; however, the magnitude of R increased. Only when R was close to 0.5, the stress state was more favorable for the fault slip, and R increased by 10%. Before the earthquake, the stresses determined through borehole QC-M-Y were in thrust fault conditions, i.e., $S_H > S_h > S_V$; however, the postearthquake stress state then became favorable for the strike slip or thrust fault movement, i.e., $S_H > S_V \geq S_h$.

Borehole QC-M-Y2 was 500 m away from borehole QC_M-Y, and the two were at approximately the same elevation; additionally, underground water levels in the two boreholes were 56 (QC-M-Y2) and 28 m (QC-M-Y). These boreholes were in the same geological unit with the same lithology; but the stress measurement campaigns were conducted before and after the earthquake. Therefore, comparing the stress data from two similar boreholes may provide valuable information. After analysis, it is observed that the stress magnitudes from borehole QC-M-Y2 were to some degree less than those from borehole QC-M-Y. The percentage decreases of k_{Hmax}, k_{hmin}, and μ_m determined after the earthquake were 12.24%, 10%, and 18.7%, respectively, which were similar to the decrease tendency of the repeated measurement obtained from borehole QC-M-Y after the earthquake. However, the decrease in amplitudes estimated with the data from borehole QC-M-Y2 was smaller than that from borehole QC-M-Y, but R increased by 11.3% with respect to the pre-earthquake value estimated from borehole QC-M-Y. The measurement results after the earthquake are similar for both boreholes. At the same time, the stress state determined by borehole QC-M-Y2 is that of thrust or strike slip conditions, i.e., $S_H > S_h \geq S_V$.

Stress measurement campaigns were conducted in four boreholes in Guangyuan precinct in the footwall of the Longmenshan fault belt from December 2007 to April 2008. After the earthquake, stress measurements were obtained from one borehole on May 23, 2008. All the boreholes contained sedimentary rock; thus, the stress measurement results can be compared with each other. These results are shown in Tables 1 and
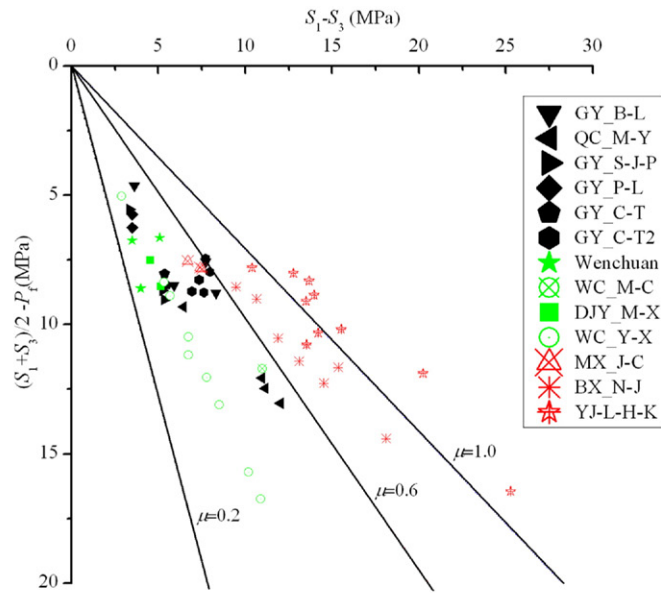
(a) Shear stress vs. mean normal stress based on the stress data in Table 1; black, green, and red denote northern, middle, and southern segments, respectively.
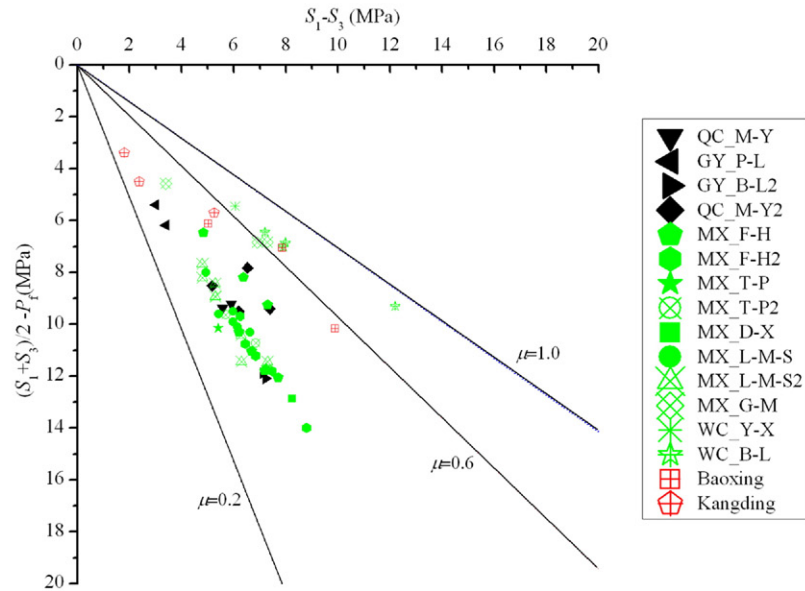
(b) Shear stress vs. mean normal stress based on the stress data in Table 2; black, green, and red denote northern, middle, and southern segments, respectively.

Fig. 6. Relation between shear stress and mean normal stress obtained from the measured stress values. (a) Shear stress vs. mean normal stress based on the stress data in Table 1; black, green, and red denote northern, middle, and southern segments, respectively. (b) Shear stress vs. mean normal stress based on the stress data in Table 2; black, green, and red denote northern, middle, and southern segments, respectively.

2. The calculated parameters were plotted on the same figure to compare the variation before and after the earthquake Fig. 8. As seen from the figure, before the earthquake, the stress data from three of the five boreholes reflected thrust–fault stress conditions, and the other two exhibited strike slip fault stress conditions. After the earthquake, however, the stress data from one borehole indicated strike slip stress conditions. The values of k_{Hmax}, k_{hmin}, μ_m, and R obtained from the six boreholes changed slightly before and after the earthquake. This lack of remarkable stress change may be attributed to the location of the measurement sites. The measurement sites are on the footwall, where the stress state is more stable than on the hanging wall; conversely, the measurement sites are tens of kilometers away from the surface rupture; hence, the earthquake may have had little influence on the stress in these sites. In fact, research on

the spatial distribution of landslides triggered by the Wenchuan Earthquake also indicated that distance from the causative faults was one of the two major factors linked to the occurrence of landslides (Qi et al., 2010). Therefore, distance from the seismogenic fault is a key factor when investigating earthquake-caused changes.

5. Discussion

5.1. Geodynamic significance of stress changes

In the previous section, we discussed our repeated measurement results from one borehole in Muyu village, Qingchuan County, in the northern segment of the Longmenshan fault belt, and observed that
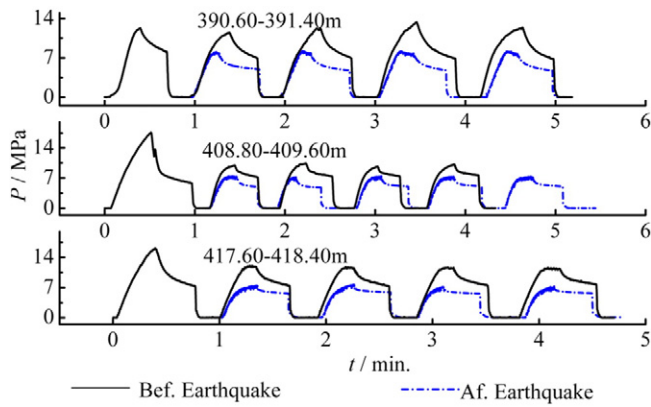
Fig. 7. Original recording curves of hydraulic fracturing in situ stress measurements before and after the earthquake.

the stress magnitudes decreased after the earthquake. During 2001 and 2002, repeated stress measurement campaigns were conducted on the seismogenic fault belt before and after the Ms 8.1 Kunlun Earthquake (Liao et al., 2003). According to Liao et al. (2003), the stress magnitudes defined after the Kunlun Earthquake were only one-third of those determined before the earthquake, and the percentage decreases of k_{Hmax}, k_{hmin}, and μ_m after the earthquake were 73%, 74%, and 19%, respectively, at one site and 67.6%, 72.4%, and 20%, respectively, at the second site. The decreases in amplitudes for the two test sites are similar; however, the decrease in amplitude after the Kunlun Earthquake was considerably higher than at the QC_M-Y test site after the Wenchuan Earthquake. The depth of the stress test interval adopted by Liao et al.(2003) was considerably less than the 100 m acceptable depth recommended by Zoback (2007). At a depth of 100, the measured stresses are seldom affected by surface topography; therefore, the measurement results may have been influenced by landforms and surface erosion (Haimson, 2010). In addition, the accumulated stresses in the surface rock mass would be released quickly, as per the findings of Li and Liu (1986). For μ_m, the decreases in amplitudes were similar for the two test sites after the Wenchuan and Kunlun earthquakes.

Tanaka et al. (1998) conducted several stress measurement campaigns near the epicentral area before the Hyogo Earthquake in Japan (January 1995, Ms 7.2) and demonstrated that the stresses increased gradually. To track the stress variation after the earthquake, two hydraulic fracturing stress measurement campaigns were undertaken in the same boreholes at two test sites, Hiragi and Heirloom.
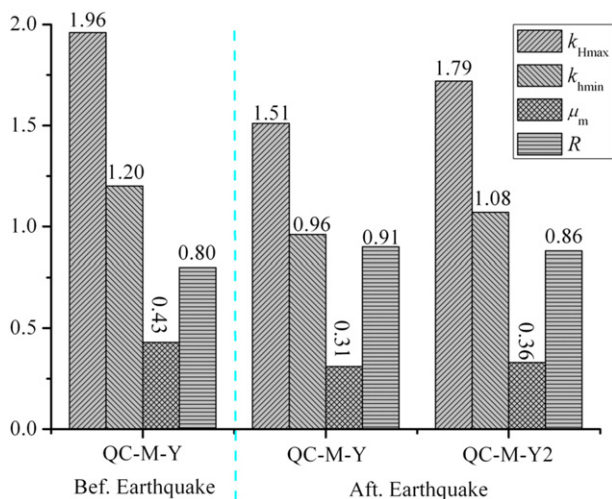
The results before and after the earthquake showed that the stresses decreased significantly after the earthquake, as shown in Fig. 9. From the results of Tanaka et al. (1998), the values of μ_m at Hiragi and Heirloom tended to increase before the earthquake and reached 0.6 at the end of 1994. However, after the Hyogo Earthquake, μ_m decreased to 0.2 and the shear stresses decreased to the common level well before the earthquake. The percentage decrease of μ_m was up to 66.7%, which is substantially higher than those values estimated after the Wenchuan and Kunlun earthquakes.

The comparison of measurements obtained before and after these three great earthquakes demonstrates that the stress decrease after the Wenchuan Earthquake was less than those after the Kunlun (Liao et al., 2003) and Hyogo (Tanaka et al., 1998) earthquakes. This is attributed to surface rupture range and changes in CFS. According to the post-earthquake geological investigation, the Ms 8.0 Wenchuan Earthquake ruptured the middle to northeastern segments of the central fault (Yingxiu-Beichuan fault) and the middle segment of the front-range fault of the Longmenshan fault belt. This created a coseismic surface rupture zone with a total length of approximately 240 km that extended approximately 15 km along the fault zone from west-southwest of Dujiangyan to southeast of Pingwu or southwest of Qingchuan (Xu et al., 2008). Inversions based on InSAR and GPS data on the coseismic surface ruptures (Feng et al., 2010; Hao et al., 2009; Tong et al., 2010) verified the field investigation results. There were no visible coseismic surface ruptures in Muyu village, Qingchuan County. Coseismic surface ruptures are always a major form of stress release after a great earthquake. Repeated measurements obtained from the second borehole QC_M-Y2 in Muyu village, close to the borehole QC_M-Y, also indicated a small stress decrease after the earthquake. Stress decreases are ongoing after the Wenchuan Earthquake, as there have been a number of aftershocks under this area (Huang et al., 2008). Considering changes in CFS as an alternate reason for the stress decrease, the Wenchuan Earthquake is believed to have increased CFS with a magnitude of 0.03–0.06 MPa on the Qingchuan fault, close to the northern end of the coseismic surface rupture (Shan et al., 2009; Toda et al., 2008; Xie et al., 2010; Zhu and Wen, 2010). Therefore, it is concluded that the stresses on the northern segment of the Longmenshan fault belt have not been released completely by the Wenchuan Earthquake.

By the comparison of these three strong earthquakes, it is found that the stress buildup before an earthquake and the stress release after an earthquake can be evaluated in the shallow crust using hydraulic fracturing in-situ stress measurement. Thus, long-term repeated stress measurements in a specific site can be utilized to monitor stress changes in the shallow crust at a potential seismic epicenter. The results for the
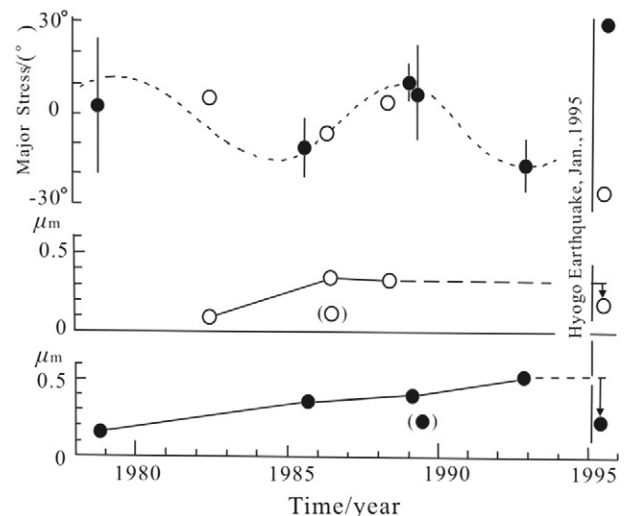

Fig. 8. Comparison of in situ stresses of two measurement sites before and after the earthquake.

Fig. 9. Variation in μ_m vs. time before and after the Hyogo Earthquake in Japan. From Tanaka et al. (1998).

three earthquakes discussed above demonstrated that μ_m, the frictional characteristic index, is a good indicator of stress buildup in the shallow crust, and hence can provide valuable information about pre-earthquake stress buildups. This knowledge is valuable for predicting earthquakes in potentially seismic regions.

5.2. Frictional strength of the Longmenshan fault belt

The stress accumulation of the upper crust agrees well with the range defined by Byerlee's law (Chang et al., 2010; Hickman and Zoback, 2004; Reasenberg and Simpson, 1992; Zoback et al., 1993). In fact, there is a rather large gap between the real value of μ calculated from measured stresses and the ideal value of $\mu = 0.6$–1.0 during the stress buildup process in the upper crust. Zoback and Healy (1984) and Townend and Zoback (2000) investigated the ratio of shear stress to normal stress on the fractures at numerous research sites, and showed that only 10%–20% of data approaches or exceeds the limit defined by $\mu = 0.6$; most values were lower than this value. Chang et al. (2010) investigated the relation between measured stresses and data of active faults, concluding that the stress magnitudes are inversely related to the activity of regional faults. From the stress data collected by Chang et al. (2010), μ_m values in thrust, strike–slip, and normal faulting areas in the South Korea Peninsula were 0.27, 0.23, and 0.11, respectively, and the average value was 0.20. Jamison and Cook (1980) estimated μ_m values from 50 sets of stress data among which the largest depth was 1900 m; the μ_m values based on stress data of thrust, strike–slip, and normal faulting conditions were 0.62, 0.22, and 0.43, respectively, and the average was 0.52. The SAFOD (San Andreas Fault Observatory at Depth) program obtained many stress measurements from several deep boreholes. Analyses of these data by the method suggested in this paper gave a mean μ_m value of 0.56 on the basis of pilot hole measurements (Hickman and Zoback, 2004). Similarly, the mean μ_m values based on measurements in two deep boreholes in the Cajon Pass (Healy and Zoback, 1988; Zoback and Healy, 1992) were 0.59 and 0.60, respectively. The slip movement speed of the regional San Andreas Fault near the Cajon Pass has been 24.5 ± 3.5 mm/a over the past 100 years (Meisling and Weldon, 1982). After the 1995 Hyogo-ken Nanbu Earthquake, in addition to the research conducted by Tanaka et al. (1998), three research boreholes were drilled in Nojima-Hirabayashi, Iwaya, and Kabutoyama along the Nojima fault, and hydraulic fracturing measurement campaigns were conducted in these boreholes (Ikeda et al., 2001); the mean μ_m values based on the measurements were 0.32, 0.34, and 0.33, respectively. All findings obtained across various locations indicated that μ_m ranges from 0.1 to 0.6, reflecting the geodynamic behaviors of different areas. In conclusion, μ_m is a potentially important geodynamic indicator for future research. From the above discussion, μ_m values within the range of 0.5–0.6 indicate a high stress buildup in the shallow crust, implying that earthquakes will occur in region of stress buildup.

In Section 4.1, the geodynamic meaning of μ_m values was discussed in terms of stress measurements along the Longmenshan fault belt. Consistent with previous studies, the μ_m values reflected not only the stress buildup along the Longmenshan fault belt, suggesting that the shallow crust is in a critical or sub-critical equilibrium state (i.e., $\mu_m = 0.30$–0.67), but also indicated the frictional strength of different segments of the Longmenshan fault. Verberne et al. (2010) investigated the static friction coefficients of fault gouge specimens obtained at the Bajiaomiao outcrop on the Yinxiu–Beichuan fault after the Wenchuan Earthquake under normal pressures of 58 to 73 MPa and temperatures of 25 to 150 °C; the corresponding friction coefficient was 0.40. Zhang and He (2013) investigated the static friction coefficients of fault gouge specimens obtained at Zhaojiagou, which is an exploratory trench on the bank of the Baisha River and Pingxi outcrops on the Yinxiu–Beichuan fault after the earthquake under normal pressures of 38 to 68.5 MPa and temperatures of 25 to 150 °C. The corresponding friction coefficients at the three outcrops were 0.20–0.22, 0.40–0.42, and 0.30–0.63. Peng et al.

(2011) performed anelastic strain recovery (ASR) tests using cores obtained from the Wenchuan Scientific Drilling Program. The mean μ_m value based on the ASR stress data was 0.37, which coincides with the range of μ_m values calculated using hydraulic fracturing stress measurements. A comparison of the friction coefficient determined by laboratory static friction tests and the μ_m values calculated using field measurements indicates that these two types of data are closely linked and fall within almost the same range. This proves that the shallow crust of the research area is in a state of frictional equilibrium, and that both data types indicate the frictional strength of regional faults.

Townend (2006) suggested that focal mechanism solution (FMS) data can be used to estimate the frictional strength of a regional fault using the Mohr–Coulomb theory. Therefore, existing FMS data were used to analyze the frictional strength of the Longmenshan fault belt and further verify previous results. Yu et al. (2010) investigated the properties and structures of different segments of the Longmenshan fault belt using FMS data for the Wenchuan Earthquake and its aftershocks. By using the FMS and fault geometry data provided by Yu et al. (2010) and the method proposed by Townend (2006), the frictional strength of five sections of the Longmenshan fault belt was estimated at four depth levels, as shown in Table 3.

The Hongkou, Longmenshan, and Chaping sections described in Table 3 belong to the middle segment of the Longmenshan fault belt investigated in this paper. The Nanba section is part the northern segment of the fault belt. The friction coefficient of faults in the shallow crust (0–5 km) based on calculations from the FMS data ranged from 0.4 to 0.6; in particular, the friction coefficient at the epicenter was as high as 0.56. For depths of 5 to 13 km, the coefficient ranged from 0.3 to 0.5, and the friction coefficient of the northern segment was higher than that of the middle segment. For depths of 13 to 19 km, the friction coefficient decreased significantly, particularly at the Longmenshan section (to 0.2); however, the coefficient only decreased slightly in the northern segment. Overall, the friction coefficients in the northern segment remained fairly stable at different depths. The friction coefficients based on the thrust faulting FMS were all greater than 0.45, indicating a medium to slightly high frictional strength for the northern segment. However, the frictional strength of the middle segment was slightly higher at shallow depths, and declined as the depth increased. Furthermore, the friction coefficient was stable at 0.2 to 0.3, indicating a low to medium frictional strength of the middle segment at a great depth and a high frictional strength at shallow depths. For an overview of the Longmenshan fault belt, all the frictional parameters based on hydraulic fracturing measurements, laboratory static friction tests, and focal mechanism data are plotted together in Fig. 10. A synthetic analysis of Fig. 10 shows that the frictional strength of the Longmenshan fault can be divided into three segments of which the southern segment is the strongest, the middle segment is the weakest, and the northern segment has intermediate strength.

Additionally, information on the frictional strength of the Longmenshan fault is useful for investigating the faulting mechanism of the Wenchuan Earthquake. In the past 2000 years, many Ms 6.0 and larger earthquakes have occurred in the middle and northern segments of the Longmenshan fault belt; however, fewer strong earthquakes occurred in the southern segment, suggesting that the background conditions of the middle and northern segments are more favorable for earthquakes. The higher frictional strength of the southern segment, in our opinion, is the main reason for fewer larger earthquakes on the southern segment relative to the middle and northern segments. At the same time, this phenomenon shows that the frictional strength controls the stress state of different segments along the Longmenshan fault belt, which is in agreement with the conclusion of Chang et al. (2010). The northeastern extension of surface ruptures from the epicenter during the Wenchuan Earthquake can be regarded as proof of the above result, i.e., the surface rupture ran through weaker crust. According to a seismogenic explanation provided by Zhang et al. (2009a,b, 2010), the nucleation location of the Wenchuan Earthquake is not in a shallow

Table 3
Fault geometries and frictional coefficients based on the focal mechanism solution data (from Yu et al, 2010).

Research area	Depth of 0–5 km			Depth of 5–13 km			Depth of 13–19 km			Depth > 19 km		
	Dip	μ_{TF}	μ_{SS}	Dip	μ_{TF}	μ_{SS}	Dip	μ_{TF}	μ_{SS}	Dip	μ_{TF}	μ_{SS}
HKSS (Epicenter)	66° ± 10°	0.56	0.54	~41°	0.38	0.41	~33°	0.39	0.31	0–16°	<0.1	0.39
LMSS (Qingping b)	~70°	0.45	0.46	60°–70°	0.49	0.5	27°	0.2	0.23	0–27°	0.2	0.25
LMSS (Hanwang b)	58°	0.47	0.45	33°	0.38	0.3	27°	0.2	0.23	0–27°	0.2	0.22
CPSS	52° ± 17°	0.43	0.39	37°–62°	0.44	0.45	37°–62°	0.48	0.42	0°?	/	/
NBSS	70°	0.5	0.41	55°–62°	0.5	0.44	37°–47°	0.45	0.32	47°?	0.56?	0.3?

Notes: (1) "?" indicates that the dip angle of the fault is uncertain when the depth is greater than 19 km, and "/" indicates that FMS data are unavailable; (2) TF = thrust fault, SS = strike–slip fault.

area of the Longmenshan fault belt but instead under the Songpan-Ganzi orogenic belt (Wang et al., 2010) to the west of the surface area of the Longmenshan fault belt. GPS observations obtained prior to the earthquake show that horizontal and vertical displacements along the Longmenshan fault belt are very small (Zhang et al., 2009a,b, 2010); however, leveling survey results indicate that there is pronounced uplift in the Songpan-Ganzi orogenic belt. Viscoelastic modeling of stress accumulation in the Longmenshan fault belt further demonstrates that the stress increase rate is larger at greater depths in the upper crust in this area (Liu et al., 2012). These findings imply that the surface middle segment of the Longmenshan fault belt is not the location of stress accumulation but instead the area of stress release and coseismic surface rupture. The fact that the stresses at the southern and northern segments of the Longmenshan fault belt are rather high implies that the southern and northern end zones of the fault belt are extremely important areas of stress concentration and transformation, and that the stress release at the two locations is not very large.

In addition to enhancing understanding of the Wenchuan Earthquake, the insights on stress changes before and after a great earthquake and μ_m based on the in situ stress measurements presented in this study have other potential engineering applications. For example, support or prevention design criteria for facilities such as pipelines, tunnels, and slopes require estimates of the amounts of stress change before and after an earthquake when the facility is located in a meizoseismal area. The cases in this paper provide reference values for stress changes for an earthquake of similar magnitude. For most applications, the findings for the Wenchuan Earthquake provide a conservative mean value for stress changes. For stress buildup and the friction strength of faults, μ_m can be used as an indicator to predict the possible stress state from the regional

seismic events and focal mechanism data in engineering areas for which stress measurements are not available. The μ_m range of 0.2 to 0.5 could provide upper and lower boundaries for future predictive analysis.

6. Conclusions

From the comparison and analysis of stress measurements along the Longmenshan fault belt obtained over 10-year period spanning before and after the Wenchuan Earthquake, the following conclusions were obtained:

(1) The in situ stress state of the Longmenshan fault belt can be divided into three segments: northern, middle, and southern. The orientation of the maximum horizontal stress rotates counterclockwise, i.e., the orientation turns from north-northwest in the northern segment to northwest in the middle segment, and to west-northwest in the southern segment. The stress magnitudes are higher in the end segments than that in the middle segment.

(2) Analyses of stress data along the Longmenshan fault belt using modified Sheorey's model and the calculated μ_m values indicate a significant stress decrease after the Wenchuan Earthquake. In addition, the stress measurement results from two boreholes in the northern segment of the Longmenshan fault belt in Muyu village, Qingchuan County before and after the earthquake indicate a fairly significant stress change in the shallow crust after the earthquake, with estimated percentage decreases of 23%–29%.

(3) μ_m is a good indicator of the regional stress buildup and frictional strength of regional faults, and in general, is in the range of 0.1–0.5. The mean μ_m value of the Longmenshan fault belt,
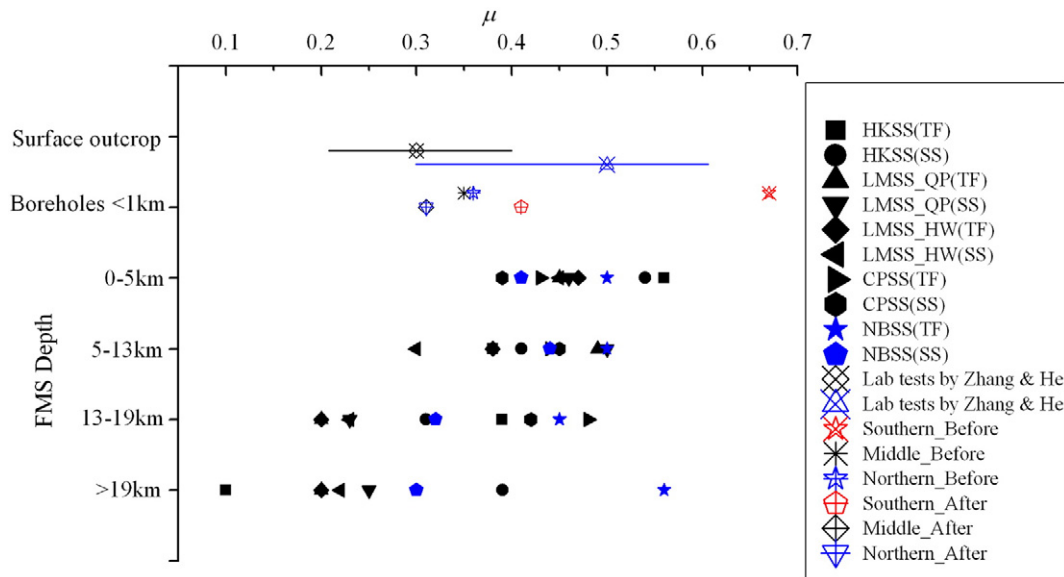
Fig. 10. Frictional strength of the Longmenshan fault at different depths based on field measurement data, laboratory test results, and FMS data (red, black, and blue denote the southern, middle, and northern segments, respectively).

calculated using field stress measurement data, is in the range of 0.46–0.36. The μ_m values based on the stress measurements further indicate that the Longmenshan fault belt can be divided into three different segments in terms of the frictional strength: a strong southern segment, weak middle segment, and a moderately strong northern segment. This finding was verified by laboratory static friction tests, FMS data, and the seismic surface rupturing process of the Wenchuan Earthquake.

(4) Analyses of the in situ stress data along the Longmenshan fault belt and the seismogenic processes of the Wenchuan Earthquake indicate that the northern and southern segments may be extremely important stress concentration and transformation nodes for the regional stress regime. In these regions, the stress characteristics are completely different from those of the middle segment. The surface area of the middle segment of the Longmenshan fault belt is not an area of stress buildup, but instead an area of stress release and surface rupture for the Wenchuan Earthquake.

The hydraulic fracturing in situ stress measurement data were restricted by the test method, personnel, and test conditions, resulting in rather scattered measurement results. These measurement data provide the information on crustal dynamics and other additional factors. Utilizing the in situ stress data to analyze the geodynamic characteristics of a great earthquake may be the most direct and effective means of understanding an earthquake. In the future, μ_m, as an index of frictional characteristics for regional faults, and as an indicator of stress buildup in regional shallow crust should be applied to other seismically active regions in the world. At present, there is still no ideal method of estimating the deep frictional strength of seismogennic fault using focal mechanism data. Much work remains to be done in this area because the frictional strength of faults is extremely important for understanding the nucleation processes of great earthquakes.

Acknowledgments

Appendix A

The apparent friction coefficient μ on a fault plane equals the ratio of shear stress to normal stress. When a fault plane is moving, the apparent friction coefficient on the fault plane can be regarded as the real friction coefficient.

$$\mu = \tau/\sigma_n \quad \text{or} \quad \mu = \tau/(\sigma_n - P_f) \tag{A.1}$$

According to the Byerlee–Anderson theory, for different types of faults, the equations for shear and normal stresses on the fault plane can be expressed as follows:

$$\text{For a thrust fault}: \tau = \frac{S_H - S_V}{2}\sin 2\alpha, \ \sigma_n = \frac{S_H + S_V}{2} - \frac{S_H - S_V}{2}\cos 2\alpha \tag{A.2}$$

$$\text{For a normal fault}: \tau = \frac{S_V - S_h}{2}\sin 2\alpha, \ \sigma_n = \frac{S_V + S_h}{2} - \frac{S_V - S_h}{2}\cos 2\alpha \tag{A.3}$$

$$\text{For a strike-slip fault}: \tau = \frac{S_H - S_h}{2}\sin 2\alpha, \ \sigma_n = \frac{S_H + S_h}{2} - \frac{S_H - S_h}{2}\cos 2\alpha. \tag{A.4}$$

Furthermore, for different types of faults, μ should be as follows:

$$\text{For a thrust fault}: \ \mu = \frac{(S_H - S_V)\sin 2\alpha}{(S_H + S_V) - (S_H - S_V)\cos 2\alpha - 2P_f} \tag{A.5}$$

$$\text{For a normal fault}: \ \mu = \frac{(S_V - S_h)\sin 2\alpha}{(S_V + S_h) - (S_V - S_h)\cos 2\alpha - 2P_f} \tag{A.6}$$

$$\text{For a strike-slip fault}: \ \mu = \frac{(S_H - S_h)\sin 2\alpha}{(S_H + S_h) - (S_H - S_h)\cos 2\alpha - 2P_f}. \tag{A.7}$$

According to the above three equations, the apparent friction coefficient is not only relevant to stress magnitudes but also depends on pore pressures. When $\mu > 0.6$, the strength of the fault is equivalent to that of the surrounding crust; when $0.6 > \mu > 0.3$, the strength of the fault is medium, and when $\mu < 0.3$, the strength of fault is weaker than that of the surrounding crust.

The fracturing process in the crust is very complicated; however, from the macro analysis of these phenomena, an increasing shear stress is the driving force for a fault slip, and the controlling resistance force is the normal stress on the fault plane. Therefore, the ratio of maximum shear stress $(S_1 - S_3)/2$ to the mean principal stress $(S_1 + S_3)/2$, μ_m, is also a parameter that describes the failure state of the crust. Townend and Zoback (2000) thought that the crust was in a critical equilibrium state, and that the stress state was stable or relatively stable, through the movements of faults and seismic events. Under critical stress conditions, the ratio of differential stress to the mean principal stress should be within a stable range. From another angle, μ_m also reflects the buildup level of regional stresses. The greater the μ_m, the higher the stress buildup, and vice versa. When the stress buildup reaches a certain level, the stress is released through fault movements so as to keep a stable crust. μ_m can reflect the strength of faults with regard to the angle of regional stress buildup; a high stress buildup level implies high strength of the regional faults.

If the role of pore pressures is considered, μ_m can be expressed as follows:

$$\mu_m = \frac{S_1 - S_3}{S_1 + S_3 - 2P_f}. \tag{A.8}$$

With respect to the previous discussion, when faults fail, the relationships between the three principal stresses can be expressed as follows:

$$S_1 - S_3 = \frac{\mu}{\sin 2\alpha + \mu \cos 2\alpha}(S_1 + S_3 - 2P_f), \tag{A.9}$$

$$\text{i.e.,} \ \mu_m = \frac{\mu}{\sin 2\alpha + \mu \cos 2\alpha}. \tag{A.10}$$

If the fault meets the requirements of the Byerlee–Anderson theory, then $\alpha = \frac{\pi}{4} - \frac{\varphi}{2}, \varphi = \tan^{-1}\mu$, and $\sin 2\alpha = \frac{1}{\sqrt{1+\mu^2}}$, $\cos 2\alpha = \frac{\mu}{\sqrt{1+\mu^2}}$; therefore, there exists a certain rule between μ_m and μ as follows:

$$\mu_m = \frac{\mu}{\sqrt{1+\mu^2}}. \tag{A.11}$$

References

Aki, K., 1984. Asperities, barriers, characteristics earthquakes and strong motion prediction. J. Geophys. Res. 89 (B7), 5867–5872.

Amadei, B., Stephansson, O., 1997. Rock Stress and its Measurement. Chapman & Hall, London.

Anderson, E.M., 1951. The Dynamics of Faulting and Dyke Formation with Applications to Britain. Edinburgh, Oliver and Boyd, Scotland.

Batchelor, A.S., 1984. Hot dry rock geothermal exploitation in the United Kingdom. Mod. Geol. 9, 1–41.

Brown, E.T., Hoek, E., 1978. Trends in relationship between measured in-situ stresses and depth. Int. J. Rock Mech. Min. Sci. 15 (8), 211–215.

Cai, C., Yu, C., Tao, K., Hu, X., Tian, Y., Zhang, H., Cui, X., Ning, J., 2011. Spatial distribution and focal mechanism solutions of the Wenchuan Earthquake series: results and implications. Earthq. Sci. 24 (1), 115–125.

Chang, C., Lee, J.B., Kang, T., 2010. Interaction between regional stress state and faults: complementary analysis of borehole in situ stress and earthquake focal mechanism in southeastern Korea. Tectonophysics 485, 164–177. http://dx.doi.org/10.1016/j.tecto.2009.12.012.

Chang, C., Jo, Y., Oh, Y., Lee, T.J., Kim, K.Y., 2014. Hydraulic fracturing in situ stress estimations in a potential geothermal site, Seokmo Island, South Korea. Rock Mech. Rock. Eng. 47 (5), 1793–1808.

Cui, X., Hu, X., Yu, C., Tao, K., Wang, Y.H., Ning, J.Y., 2011. Research on focal mechanism solutions of Wenchuan Earthquake sequence. Acta Sci. Nat. Univ. Pekin. 47 (6), 1063–1072.

Deng, Q., Chen, S., Zhao, X., 1994. Tectonics, seismicity and dynamics of Longmenshan mountains and its adjacent regions. Acta Seismol. Sin. 16 (4), 389–403.

Densmore, A.L., Ellis, M.A., Li, Y., Zhou, R., Hancock, G.S., Richardson, N., 2007. Active tectonics of the Beichuan and Pengguan faults at the eastern margin of the Tibetan Plateau. Tectonics 26 (4). http://dx.doi.org/10.1029/2006TC001987 (TC 4005).

Department of earthquake monitoring and prediction of CEA, 2009. Scientific Research Report on the Wenchuan Ms. 8.0 Earthquake. Earthquake Publish Company, Beijing.

Diao, G., Xu, X., Chen, Y., Huang, B., Wang, X.S., Feng, X.D., Yang, Y.Q., 2011. The precursory significance of tectonic stress field transformation before the Wenchuan M_w 7.9 Earthquake and the Chi-Chi M_w 7.6 Earthquake. Chin. J. Geophys. 54 (1), 128–136 (in Chinese).

Ding, Z., Wu, Y., Wang, H., Zhou, X., Li, G., 2008. Variations of shear wave splitting in the 2008 Wenchuan Earthquake region. Sci. China Ser. D Earth Sci. 51 (12), 1712–1716.

Feng, G., Hetland, E.A., Ding, X., Li, Z., Zhang, L., 2010. Coseismic fault slip of the 2008 M_w 7.9 Wenchuan Earthquake estimated from InSAR and GPS measurements. Geophys. Res. Lett. 37, L01302. http://dx.doi.org/10.1029/2009GL041213.

Gan, W., Zhang, P., Shen, Z.K., Niu, Z., Wang, M., Wan, Y., Zhou, D., Cheng, J., 2007. Present-day crustal motion within the Tibetan Plateau inferred from GPS measurements. J. Geophys. Res. 112, B08416. http://dx.doi.org/10.1029/2005 JB 004120.

Guo, Q.L., Wang, C.H., Ma, H.S., Wang, C.G., 2009. In-situ hydro-fracture stress measurement before and after the Wenchuan Ms 8.0 Earthquake of China. Chin. J. Geophys. 52 (5), 1395–1401. http://dx.doi.org/10.3969/j (ISSN. 0001-5733.2009.05.029, In Chinese).

Haimson, B.C., 2010. The effect of lithology, inhomogeneity, topography, and faults, on in situ stress measurements by hydraulic fracturing, and the importance of correct data interpretation and independent evidence in support of results [C]. In: Xie (Ed.), Rock Stress and Earthquakes. Taylor & Francis Group, London.

Haimson, B.C., Cornet, F.H., 2003. ISRM suggested methods for rock stress estimation—part 3: hydraulic fracturing (HF) and/or hydraulic testing of pre-existing fractures (HTPF). Int. J. Rock Mech. Min. Sci. 40 (7–8), 1011–1020.

Haimson, B.C., Fairhurst, C., 1970. In Situ Stress Determination at Great Depth by Means of Hydraulic Fracturing, Rock Mechanics—Theory and Practice. In: Somerton, W.H. (Ed.), Am. Inst. Mining Engrg., pp. 559–584.

Hao, K.X., Si, H., Fujiwara, H., Ozawa, T., 2009. Coseismic surface-ruptures and crustal deformations of the 2008 Wenchuan Earthquake Mw 7.9, China. Geophys. Res. Lett. 36 (11), L11303. http://dx.doi.org/10.1029/2009GL037971.

Healy, J., Zoback, M.D., 1988. Hydraulic fracturing stress measurements in the Cajon Pass research well to 2 km depth. Geophys. Res. Lett. 15, 1005–1008.

Heidbach, O., Tingay, M., Barth, A., Reinecker, J., Kurfeß, D., Müller, B., 2008. The World Stress Map Database Release 2008. http://dx.doi.org/10.1594/GFZ.WSM.Rel2008.

Hickman, T., Zoback, M.D., 2004. Stress orientations and magnitudes in the SAFOD pilot hole. Geophys. Res. Lett. 31 (15), 12–15.

Hu, X., Yu, C., Tao, K., Cui, X.F., Ning, J.Y., Wang, Y.H., 2008. Focal mechanism solutions of Wenchuan Earthquake and its strong aftershocks obtained from initial P wave polarity analysis. Chin. J. Geophys. 51 (6), 1711–1718 (in Chinese).

Huang, Y., Wu, J.P., Zhang, T.Z., Zhang, D.N., 2008. Relocation of the M8.0 Wenchuan Earthquake and its aftershock sequence. Sci. China Ser. D 51 (12), 1703–1711. http://dx.doi.org/10.1007/s11430-008-0135-z.

Ikeda, R., Iio, Y., Omura, K., 2001. In situ stress measurements in NIED boreholes in and around the fault zone near the 1995 Hyogo-ken Nanbu Earthquake, Japan. Island Arc 10, 252–260.

Ito, T., Evans, K., Kawai, K., Hayashi, K., 1999. Hydraulic fracture reopening pressure and the estimation of maximum horizontal stress. Int. J. Rock Mech. Min. Sci. 36 (6), 811–826.

Ito, T., Igarashi, A., Kato, H., Ito, H., Sano, O., 2006. Crucial effect of system compliance on the maximum stress estimation in the hydraulic fracturing method: theoretical considerations and field-test verification. Earth Planets Space 58 (8), 963–971.

Ito, T., Satoh, T., Kato, H., 2010. Deep rock stress measurement by hydraulic fracturing method taking account of system compliance effect[C]. In: Xie (Ed.), Rock Stress and Earthquakes. Taylor & Francis Group, London.

Jamison, D.B., Cook, N.G.W., 1980. Note on measured values for the state of stress in the Earth's crust. J. Geophys. Res. 85, 1833–1838.

Kim, K., Franklin, J.A., 1987. Suggested methods for rock stress determination[C]. International Journal Of Rock Mechanics And Mining Sciences & Geomechanics Abstracts 24. Pergamon-Elsevier Science Ltd, The Boulevard, Langford Lane, Kidlington, Oxford, England Ox5 1gb, pp. 53–73.

King, G.C.P., Stein, R.S., Lin, J., 1994. Static stress changes and the triggering of earthquakes. Bull. Seismol. Soc. Am. 84, 935–953.

Lee, M.Y., Haimson, B.C., 1989. Statistical evaluation of hydraulic fracturing stress measurement parameters. Int. J. Rock Mech. Min Sci. 26 (6), 447–456.

Li, F., Liu, G., 1986. In-situ stress measurement, stress state of the upper crust and the earthquake. Earthq. China 2 (1), 50–55.

Li, C., Song, F., Ran, Y., 2004. Late quaternary activity and age constraint of the northern Longmenshan fault zone. Acta Seismol. Sin. 26 (2), 248–258.

Liao, C.T., Zhang, C.S., Wu, M.L., Ma, Y.S., Ou, M.Y., 2003. Stress change near the Kunlun fault before and after the Ms 8.1 Kunlun Earthquake. Geophys. Res. Lett. 30 (20), 2027–2030.

Lin, J., Stein, R.S., 2004. Stress triggering in thrust and subduction earthquakes and stress interaction between the southern San Andreas and nearby thrust and strike–slip faults. J. Geophys. Res. 109 (B2), 20183–20202.

Liu, C., Zhu, B.J., Shi, Y.L., 2012. Stress accumulation of the Longmenshan fault and recurrence interval of Wenchuan Earthquake based on viscoelasticity simulation. Acta Geol. Sin. 86 (1), 157–169 (in Chinese).

Ma, B.Q., Su, G., Hou, Z.H., Shu, S.B., 2005. Late quaternary slip rate in the central part of the Longmenshan fault zone from terrace deformation along the Minjiang River. Acta Seismol. Sin. 27 (2), 234–242.

Meisling, K.E., Weldon II, R.J., 1982. Slip-rate, offset, and history of the Cleghorn fault, western San Bernadino Mountains, southern California. Geol. Soc. Am. Abstr. Programs 11, 215.

Parsons, T., Ji, C., Kirby, E., 2008. Stress changes from the 2008 Wenchuan Earthquake and increased hazard in the Sichuan basin. Nature 454 (7203), 509–510. http://dx.doi.org/10.1038/nature07177.

Peng, H., Ma, X.M., Jiang, J.J., 2011. In-situ stress measurement by differential strain analysis method in WFSD-1. J. Geomech. 17 (3), 249–260 (In Chinese).

Qi, S.W., Xu, Q., Lan, H.X., Zhang, B., Liu, J.Y., 2010. Spatial distribution analysis of landslides triggered by 2008.5.12 Wenchuan Earthquake, China. Eng. Geol. 116 (1–2), 95–108. http://dx.doi.org/10.1016/j.enggeo.2010.07.011.

Reasenberg, P.A., Simpson, R.W., 1992. Response of regional seismicity to the static stress change produced by the Loma Prieta Earthquake. Science 255 (5052), 1687–1690.

Rummel, F., Möhring-Erdmann, G., Baumgärtner, J., 1986. Stress constraints and hydraulic fracturing stress data for the continental crust. Pure Appl. Geophys. 124 (4/5), 875–895.

Shan, B., Xiong, X., Zheng, Y., Diao, F.Q., 2009. Stress changes on major faults caused by Mw 7.9 Wenchuan Earthquake, May 12, 2008. Sci. China Ser. D Earth Sci. 52 (5), 593–601.

Shen, Z., Lu, J., Wang, M., Burgamann, R., 2005. Contemporary crustal deformation around the southeast borderland of the Tibetan plateau. J. Geophys. Res. 110 (B11), 1–17.

Sheorey, P.R., 1994. A theory for in-situ stress in isotropic and transversely isotropic rock. Int. J. Rock Mech. Min. Sci. Geomech. Abstr. 31 (1), 23–34.

Tanaka, Y., 1986. State of crustal stress inferred from in-situ stress measurements. J. Phys. Earth 34 (Supp. 1), S57–S70.

Tanaka, Y., Fujimori, K., Otsuka, S., 1998. In-situ stress measurement and prediction of great earthquake. Earthquake 50 (2), 201–208 (in Japanese).

Tang, C., Han, W., 1993. Active Geological Structures in Sichuan and Earthquake. Earthquake Publish Company, Beijing, p. 369.

Teng, J.W., Bai, D.H., Yang, H., Yan, Y.F., Zhang, H.S., Zhang, Y.Q., Ruan, X.M., 2008. Deep processes and dynamic responses associated with the Wenchuan Ms 8.0 Earthquake of 2008. Chin. J. Geophys. 51 (5), 1385–1402.

Toda, S., Lin, J., Meghraoui, M., Stein, R.S., 2008. 12 May 2008 Ms 7.9 Wenchuan, China, Earthquake calculated to increase failure stress and seismicity rate on three major fault systems. Geophys. Res. Lett. 35, L17305. http://dx.doi.org/10.1029/2008GL034903.

Tong, X., Sandwell, D.T., Fialko, Y., 2010. Coseismic slip model of the 2008 Wenchuan Earthquake derived from joint inversion of interferometric synthetic aperture radar, GPS, and field data. J. Geophys. Res. 115, B04314. http://dx.doi.org/10.1029/2009JB006625.

Townend, J., 2006. What do faults feel? Observational constraints on the stresses acting on seismogenic faults. Geophys. Monogr. 170, 313–327.

Townend, J., Zoback, M.D., 2000. How faulting keeps the crust strong. Geology 28 (5), 399–402.

Verberne, B.A., He, C.R., Spiers, C.J., 2010. Frictional properties of sedimentary rocks and natural fault gouge from the Longmenshan fault zone, Sichuan, China. Bull. Seismol. Soc. Am. 100, 2767–2790.

Wang, C.H., Guo, Q.L., Ding, L.F., Liu, L.P., 2009. High in-situ stress criteria for engineering area and a case analysis. Rock Soil Mech. 30 (8), 2359–2364 (In Chinese).

Wang, H., Liu, M., Shen, X., Liu, J., 2010. Balance of seismic moment in the Songpan-Ganze region, eastern Tibet: implications for the 2008 Great Wenchuan Earthquake. Tectonophysics 491 (1–4), 154–164. http://dx.doi.org/10.1016/j.tecto.2009.09.022.

Wen, X.Z., Zhang, P.Z., Du, F., Long, F., 2009. The background of historical and modern seismic activities of the occurrence of the 2008 Ms 8.0 Wenchuan, Sichuan, Earthquake. Chin. J. Geophys. 52 (2), 444–445.

Wiemer, S., Wyss, M., 1997. Mapping the frequency–magnitude distribution in asperities: an improved technique to calculate recurrence times? J. Geophys. Res. 102 (B7), 15115–15128.

Wiemer, S., Wyss, M., 2000. Minimum magnitude of completeness in earthquake catalogs: examples from Alaska, the western United States and Japan. Bull. Seismol. Soc. Am. 90 (4), 859–869.

Wu, M.L., Zhang, Y.Q., Liao, C.T., Chen, Q.C., Ma, Y.S., Wu, J.S., Yan, J.S., Yan, J.F., Ou, M.Y., 2010. Preliminary results of in situ stress measurements along the Longmenshan Fault Zone after the Wenchuan Ms 8.0 Earthquake. Acta Geol. Sin. 84 (9), 1292–1299.

Wyss, M., Matsumura, S., 2002. Most likely location of large earthquakes in the Kanto and Tokai areas, Japan, based on the local recurrence times. Phys. Earth Planet. Inter. 131, 173–184.

Wyss, M., Schorlemmer, D., Wiemer, S., 2000. Mapping asperities by minima of local recurrence time: San Jacinto-Elsinore fault zones. J. Geophys. Res. 105 (B4), 7829–7844.

Xie, F.R., Chen, Q.C., Cui, X.F., Li, H., Yang, S.X., Chen, L.W., 2003. Study on the Crustal Stress Environment of the China Mainland. Geological Publishing House, Beijing.

Xie, C.D., Zhu, Y.Q., Lei, X.L., Yu, H.Y., Hu, X.L., 2010. Pattern of stress change and its effect on seismicity rate caused by Ms 8.0 Wenchuan Earthquake. Sci. China Earth Sci. 53, 1260–1270. http://dx.doi.org/10.1007/s11430-010-4025-9.

Xu, Z., Ji, S., Li, H., Hou, L., Fu, X., Cai, Z., 2008. Uplift of the Longmenshan range and the Wenchuan Earthquake. Episodes 31 (3), 291–301.

Xu, X.W., Wen, X.Z., Yu, G.H., Chen, G.H., Klinger, Y., Hubbard, J., Shaw, J., 2009. Coseismic reverse- and oblique-slip surface faulting generated by the 2008 Mw 7.9 Wenchuan Earthquake, China. Geology 37 (6), 515–518. http://dx.doi.org/10.1130/G25462A.1.

Yamashita, F., Mizoguchi, K., Fukuyama, E., Omura, K., 2010. Reexamination of the present stress state of the Atera fault system, central Japan, based on the calibrated crustal stress data of hydraulic fracturing tests obtained by measuring the tensile strength of rocks. J. Geophys. Res. Solid Earth 115 (B4) (1978–2012).

Yu, G., Xu, X., Klinger, Y., Diao, G., Chen, G., Feng, X., Li, C., Zhu, A., Yuan, R., Guo, T., Sun, X., Tan, X., An, Y., 2010. Fault-scarp features and cascading-rupture model for the Mw 7.9 Wenchuan Earthquake, eastern Tibetan plateau, China. Bull. Seismol. Soc. Am. 100 (5B), 2590–2614. http://dx.doi.org/10.1785/0120090255.

Zang, A., Stephansson, O., 2010. Stress Field of the Earth's Crust. Springer, Heidelberg, London, New York, pp. 141–153.

Zhang, L., He, C., 2013. Frictional properties of natural gouges from Longmenshan fault zone ruptured during the Wenchuan Mw 7.9 Earthquake. Tectonophysics 594 (5), 149–164.

Zhang, P.Z., Wen, X.Z., Xu, X.W., Gan, W.J., Wang, M., Shen, Z.K., Wang, Q.L., Huang, Y., Zhen, Y., Li, X.J., Zhang, Z.Q., Ma, S.L., Ran, Y.K., Liu, Q.Y., Ding, Z.F., Wu, J.P., 2009a. Tectonic model of the great Wenchuan Earthquake of May 12, 2008, Sichuan, China. Chin. Sci. Bull. 54 (7), 944–953 (Chinese Ver, in Chinese).

Zhang, Z.W., Cheng, W.Z., Ruan, X., Wu, P., 2009b. The seismicity and tectonic stress field characteristics of the Longmenshan fault zone before the Wenchuan Ms 8.0 Earthquake. Acta Seismol. Sin. 31 (2), 117–127 (in Chinese).

Zhang, P.Z., Wen, X.Z., Shen, Z.K., Chen, J.H., 2010. Oblique, high-angle, listric-reverse faulting and associated development of strain: the Wenchuan Earthquake of May 12, 2008, Sichuan, China. Annu. Rev. Earth Planet. Sci. 38, 353–382. http://dx.doi.org/10.1146/annurev-earth-040809-152602.

Zhang, Y.S., Shi, J.S., Sun, P., Yang, W.M., Yao, X., Zhang, C.S., Xiong, T.Y., 2013. Surface ruptures induced by the Wenchuan Earthquake: their influence widths and safety distances for construction sites. Eng. Geol. 166 (8), 245–254. http://dx.doi.org/10.1016/j.enggeo.2013.09.010.

Zhou, R.J., Li, Y., Densmore, A.L., Ellis, M.A., He, Y.L., Li, Y.Z., Li, X.G., 2007. Active tectonics of the Longmenshan Region of the eastern margin of the Tibetan plateau. Acta Geol. Sin. 81 (4), 593–604.

Zhu, H., Wen, X., 2010. Static stress triggering effects related with Ms 8.0 Wenchuan Earthquake. J. Earth Sci. 21 (1), 32–41.

Zoback, M.L., 1992. First-and second-order patterns of stress in the lithosphere: the world stress map project. J. Geophys. Res. 97 (138), 11703–11728.

Zoback, M.D., 2007. Reservoir Geomechanics. Cambridge University Press, Cambridge, p. 464.

Zoback, M.D., Healy, J.H., 1984. Friction, faulting and in situ stress. Ann. Geophys. 2 (6), 689–698.

Zoback, M.D., Healy, J.H., 1992. In-situ stress measurements to 3.5 km depth in the Cajon Pass scientific research borehole: implications for the mechanics of crustal faulting. J. Geophys. Res. 97 (B4), 5039–5057.

Zoback, M.L., Magee, M., 1991. Stress magnitudes in the crust: constraints from stress orientation and relative magnitude data. Philos. Trans. R. Soc. Lond. A 337, 181–194.

Zoback, M.D., Townend, J., 2001. Implications of hydrostatic pore pressure and high crustal strength for the deformation of intraplate lithosphere. Tectonophysics 336 (1–4), 19–30.

Zoback, M.D., Apel, R., Baumgärtner, J., Brudy, M., Emmermann, R., Engeser, B., Fuchs, K., Kessels, W., Rischmüller, H., Rummel, F., Vernik, L., 1993. Upper-crustal strength inferred from stress measurements to 6 km depth in the KTB borehole. Nature 365, 633–635.